Gone Fishing: Synthesis and Design of a Superparamagnetic Nanobait for Trapping Reactive Metabolites *in vivo*.

Ehsen Tayyabi

Thesis submitted to the

Faculty of Graduate and Postdoctoral Studies

in partial fulfillment of the requirements for the

MSc degree in Chemistry

Department of Chemistry and Biomolecular Sciences

Faculty of Science

University of Ottawa

Candidate	Supervisor
Ehsen Tayyabi	Professor Adam Shuhendler

ABSTRACT

Adverse drug reactions are common causes of medical injuries. Drug-induced hepatotoxicity remains one of the leading causes of emergency room visits, FDA non-approval, and drug withdrawal from the market. We have investigated the ability of endogenous nucleophilic amino acid residues (K, H, and C) to selectively bind to reactive electrophilic drug metabolites, focusing on acetyl-*para*-aminophenol (APAP, i.e. Tylenol®), for which hepatotoxicity has recently re-emerged as a major health concern for Canadians. Three peptide sequences were synthesized bearing terminal nucleophilic residues, brominated phenylalanine residues, and c-terminal amides. These peptides were coupled to carboxy methyl dextran coated iron oxide nanoparticles (CMX-IONPs) with a hepatocyte targeting group. IONPs are known for their ability to act as T_2-weighted MRI contrast agents, giving us the ability to track them *in vivo*. This study begins to establish a nanotechnology-based method for the *in vivo* trapping of NAPQI, the reactive metabolite of APAP, using a cysteine bearing IONP.

ACKNOWLEDGEMENTS

I would like to thank Professor Adam Shuhendler for giving me the opportunity to work in his research group, and for taking me on as his first graduate student. Through my work in the Molecular Medicine group I learned a lot of important scientific skills, but most importantly I learned how to completely ignore the constant noise of construction. I would also like to thank all of the wonderful people I had the opportunity to work alongside during my graduate studies at the University of Ottawa. Special thanks go out to Yen Truong, Trina Dang, Mojmir Suchy, and Mackenzie Reid of the mol med group. Since the Marion second floor lab was an open lab I also had the opportunity of meeting fellow colleagues in the Boddy, Keillor, DaCosta, and Valois lab who had a huge impact on my graduate studies. I would like to specifically thank Professor Christopher Boddy and Professor John Pezacki for being a part of my graduate studies committee, and for their constant guidance and support.

This work would also not have been possible without the support of my family and friends, so big shout out to them.

I would also like to thank all agencies that funded my scientific work at the University of Ottawa.

In the words of the late Biggie Smalls "Stay far from timid, only make moves when your heart's in it, and live the phrase 'sky's the limit.'"

TABLE OF CONTENTS

List of Figures and Tables

1.0 Introduction and Literature Review:

1.1 Drug Induced Liver Injury:

Adverse drug reactions (ADR) are a common and dangerous complication that can lead to unpredictable life-threatening injury and can cause drug withdrawal at late stages of drug development (Bouvy, Bruin, & Koopmanschap, 2015). ADRs are defined as a harmful or unpleasant reaction from an intervention related to the use of a medicinal product, potentially causing a change of dosage, or withdrawal of the product (Edwards & Aronson, 2000). The chemical stress produced by these reactive drug metabolites is said to be the primary cause of drug-induced liver injury (DILI) (Leung et al., 2017), which is a sudden and life-threatening liver dysfunction. DILI can range from asymptomatic transaminitis to acute liver failure (ALF) or fulminant hepatic failure (FH) (Khoury et al., 2015). Severe DILI tends to be a rare clinical phenomenon, but drug-induced hepatic injury has become one of the leading causes of ALF in the United States and other western countries (Lewis, 2015). Approximately 1600 to 2000 people in the United States develop ALF per year, where 30% of them receive aggressive hepatic therapy including transplantation (*Ostapowicz* et al., 2002).

DILI is a major problem both in the clinic and for the pharmaceutical industry. Since DILI is involved in many cases of ALF and drug development is a long and expensive process, it becomes important to investigate potential toxicities at an early stage (Lewis, 2015). DILI can be divided into two major categories: intrinsic and idiosyncratic.

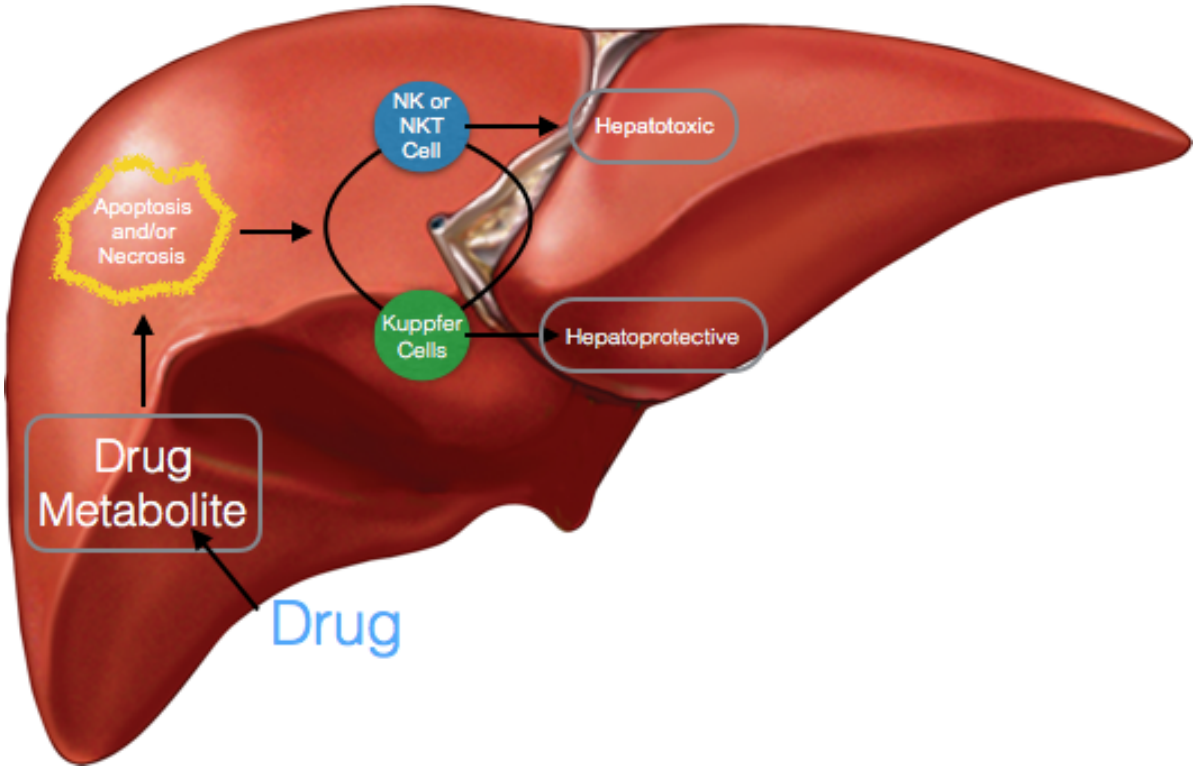

Figure 1.1: Mechanisms of Hepatic Drug Metabolism.

Drug metabolites tend to be electrophilic and hence will react with various endogenous nucleophiles or induce oxidative stress leading to cell death. In most cases the body's detoxification mechanisms will remove the metabolite via means of glutathione binding, glucuronidation, or various other mechanisms. In the case where the detoxification method is not sufficient or depleted, the metabolite can react with endogenous proteins creating protein adducts and or inducing oxidative stress. Depending on the role of these proteins and how critical they are in cellular function, this can eventually lead to an immune response causing a hepatotoxic event.

Intrinsic DILI tends to be predictable and dose dependent whereas idiosyncratic is unpredictable and not dose dependent. The most prevalent cause of intrinsic DILI is N-(4-hydroxyphenyl)acetamide (acetaminophen), leading to $87 million being spent on treating complications of overdose (Offerman, 2011). Since APAP is the leading cause of intrinsic ALF

in the United States and is an optimal drug with a well characterized metabolic pathway, it is important to better understand the role of APAP in DILI and ALF (David Josephy, 2005).

1.2 Predictive factors for DILI

There are certain host risk factors that my increase the chance of DILI such as age, gender, underlying liver disease, use of alcohol, and obesity. It was noted that DILI was more predominant in females than males which may be due to the higher dosage of hepatotoxic medications prescribed to females (Holt & Ju, 2006). Various studies were conducted in order to correlate the risk of DILI with increasing age, however there was no age correlation found for susceptibility to DILI, as there are many other factors to consider in DILI such as previous disease history (Stine, Sateesh, & Lewis, 2013). Chen et al. investigated whether DILI was caused by a one-time large dosage of a specific hepatotoxin or if even small dosages could increase the likelihood of DILI, and found that drugs that were substrates for cytochrome P450 (CYP450) tended to increase the likelihood of hepatic injury (Chen et al., 2014). This study discovered that more significant than age, lipophilicity of the hepatotoxin, and gender, the pharmacologic properties, such as enzyme targets of the specific hepatotoxin, were large indicating factors of susceptibility to DILI (Chen et al., 2014; Holt & Ju, 2006; Stine et al., 2013).

1.3 Treatment and Detection of DILI

Most drugs that have the potential to induce hepatic injury carry the warning to reduce dose if liver disease is present. However, there remains little to no scientific data supporting the notion that reducing dosage of a hepatotoxin will decrease the likelihood of DILI (Lewis, 2015). Another commonly used tool for preventing hepatic injury is the use of liver-associated biochemistry or enzyme monitoring (LAE). This monitoring process remains expensive and inconvenient, and is

not successful in most cases of DILI (Holt & Ju, 2006). LAE can only be useful for monitoring the enzymes in the liver when there is use of a drug with known risk of hepatotoxicity (Khoury et al., 2015). Conventional serum biomarkers such as alanine amino transferase (ALT), aspartate aminotransferase (AST), alkaline phosphatase (ALP) and total bilirubin (TBIL) have been routinely used to detect and manage DILI (Dukes et al., 2017). These biomarkers are traditionally good indicators of hepatic injury although cannot be utilized as indicators of DILI as they are markers of overt liver injury (Nathwani, Pais, Reynolds, & Kaplowitz, 2005). Hy's law, attributed to Dr. Hyman Zimmerman, is a guidance for hepatic injury with patients in clinical trials starting with a healthy liver whose serum levels of ALT and TBIL increase past a specific threshold. The assumption is that biomarker elevation in the serum is an indicative factor of loss of liver function due to loss of hepatocytes (Church, Watkins, & Law, 2017). A major limitation of Hy's law is that these elevations in serum proteins may be a result of various other implications such as haemolysis or changes in bilirubin transport mechanisms.

Due to these limitations research efforts have been carried out to investigate newer biomarkers of hepatic injury (Yang et al., 2017). Recent studies show that glutamate dehydrogenase (GLDH) and microRNA-122 (miR-122) may be more sensitive and specific biomarkers of liver injury than ALT. Some work has also gone into developing an "apoptotic index" (AI) based on various serum biomarkers (Church et al., 2017). The AI is a ratio of caspase cleaved keratin 18 (ccK18) to regular keratin18 (K18). During early stages of apoptosis K18 is cleaved by caspase giving ccK18, making ccK18 an adequate biomarker for early stage apoptosis (Caulín, Salvesen, & Oshima, 1997). GLDH has also been investigated as an early stage biomarker for DILI. GLDH is located in the mitochondrial matrix and is implicated in amino acid oxidation and urea production. A study

conducted by Schomaker *et al*., compared the diagnostic power of GLDH and ALT levels. It was shown the GLDH had better diagnostic potential for predicting liver injury from various aetiologies (Schomaker et al., 2013). Since the half-life of GLDH is lower than that of ALT it seems to be a better indicator of hepatic injury since less of it will be in circulation over longer periods of time and are more reflective of ongoing liver injury (Mcmillan, Gregas, Darras, & Kang, 2011).

There are certain serum biomarkers for predicting hepatic injury, but treatment of DILI remains a major obstacle as it consists of terminating treatment with the drug in question or hospital based supportive treatment. Both of these treatments have their respective obstacles. Terminating treatment may not be possible depending on the necessity of the medication and supportive treatment tends to be expensive (Leise, Poterucha, & Talwalkar, 2014). There are various conventional methods of treating hepatic injury although they possess their own limitations. The most common treatment for hepatic injury is N-Acetyl-Cysteine (NAC) but this has only been investigated in APAP induced hepatic injury (Holt & Ju, 2006). NAC was first used as a treatment for APAP overdose in 1979, where upon administration NAC replenishes GSH stores (Hazelton et al., 1986) and has remained the treatment of choice in human overdose cases of APAP for many years (Smilkstein et al., 1991).

Further investigations are now being carried out to determine if the use of NAC can possess hepatoprotective properties for treatment with other drugs. In a randomized clinical trial in comparing adults with non-APAP induced liver injury NAC was associated with mortality benefit (Larson, Ii, Murray, Mccashland, & Reisch, 2009). Another study investigated the use of NAC

for treatment of non-APAP induced hepatic failure in paediatric patients and it was shown the administration of NAC had decreased hospital stay and improved survival (Chughlay et al., 2015). Since current therapies are quite limited in treating hepatic injury, investigating mechanisms of hepatic injury will help in the development of better and more specific therapies for DILI.

1.4 Implications of DILI in Drug Development

Our understanding of the mechanisms of DILI remain limited, and there remains a need for new methodologies to help in the drug development process, specifically to investigate the role of reactive metabolites *in vivo* (Park et al., 2011). It is proposed that reactive metabolites of these drugs play a role in many cases of DILI through covalent and functional perturbation of proteins. Another mechanism of toxicity may be through immunogenic responses by generating drug-derived antigens (Uetrecht & Naisbitt, 2013). The drug industry has various mechanisms in place to determine apparent drug safety through *in vitro* screens of reactive metabolites and protein drug metabolite adducts. In some cases, the industry labels compounds as "structural alerts" where the compound in its entirety is avoided due to the potential of producing reactive metabolites (Dalvie, Kalgutkar, & Chen, 2017). A more meaningful way of assessing potential drug toxicity may involve incorporating factors such as drug dose, alternative metabolic routes, and risk- benefit related indications. The latter method provides promise but requires a better understanding of the reactivity of certain drugs *in vivo* and a method to characterize their behaviour in living subjects (Whitby, Obach, Simon, Hayward, & Cravatt, 2017).

Investigations have been conducted in order to determine whether all protein-metabolite adducts produce toxic effects. Modifications to parent compounds, such as in the case with APAP, showed

that analogues of the drug produced metabolite-protein adducts although did not display the hepatotoxic effects of the parent drug, as seen in figure 1.2 (Matthewsa, Hinson, Robertsa, & Pumford, 1997).

Protein-covalent binding is in most cases measured via radiolabelling of the parent molecule followed by quantifying the amount bound to bulk protein or cellular components. A major limitation of this process is that it does not identify the site-specificity of the protein adducts formed and the quantity of protein adducts formed does not always correlate with the severity of the toxicity (Evans, Watt, Nicoll-griffith, & Baillie, 2004).

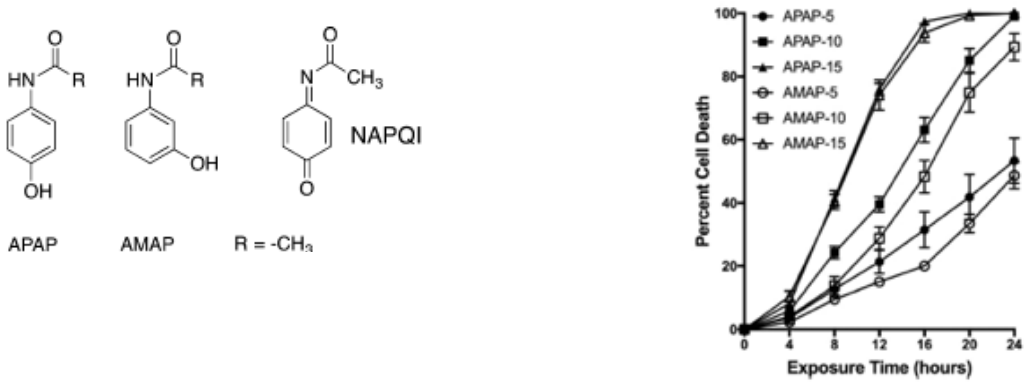

Figure 1.2: Modifications to APAP and their effect on toxicity.
Analogues of APAP have different outcomes compared to the parent compound. As seen here AMAP analogues showed less percentage cell death when compared to APAP analogues, suggesting that the presence of the quinoneimine is responsible for toxicity. This data supports the claim that changing molecular structure even slightly may change its potency as a drug, but the toxicity can still be present if the metabolic product produced is electrophilic and reactive such as in the case of NAPQI. 5,10, and 15 refer to increasing concentrations of the respective compound compared to the recommended dosage. Reproduced from Koen, Liu, Shinogle, Williams, & Hanzlik, 2016 (Comparative Toxicity and Metabolism of N-Acyl Homologues of Acetaminophen and Its Isomer 3'-Hydroxyacetanilide)

Structural modifications may be implemented during the lead optimization of drug development to limit the extent of reactive metabolite production. Initial optimization can be done by using

trapping agents such as glutathione and cyanide in order to characterize protein-drug adducts (Evans et al., 2004).

1.5 Mechanism of Hepatic Injury

Reactive metabolites can cause DILI through a variety of mechanisms such as glutathione depletion, binding enzymes, lipids, nucleic acids, and other cell structures. The majority of reactive metabolites are formed through phase I oxidation but phase II metabolic products and parent drugs can induce hepatic injury as well (Holt & Ju, 2006). Ultimately DILI research is premised around three main components: toxic electrophilic metabolites of drugs, bound proteins in target cells, and the biochemical consequence of binding (Evans et al., 2004). Protein binding to electrophilic metabolites can either be protective or destructive depending on the importance of the protein binding and the localization of the protein-drug adduct.

Protective measures can be carried out when the protein plays a non-critical role in cellular function and can pass as a beacon for reducing reactive metabolite concentrations in the hepatocyte. Alternatively, destructive measures are observed when the metabolite-modified protein serves a critical role in cellular function, ultimately compromising its activity (Chandrasekharan et al., 2002).

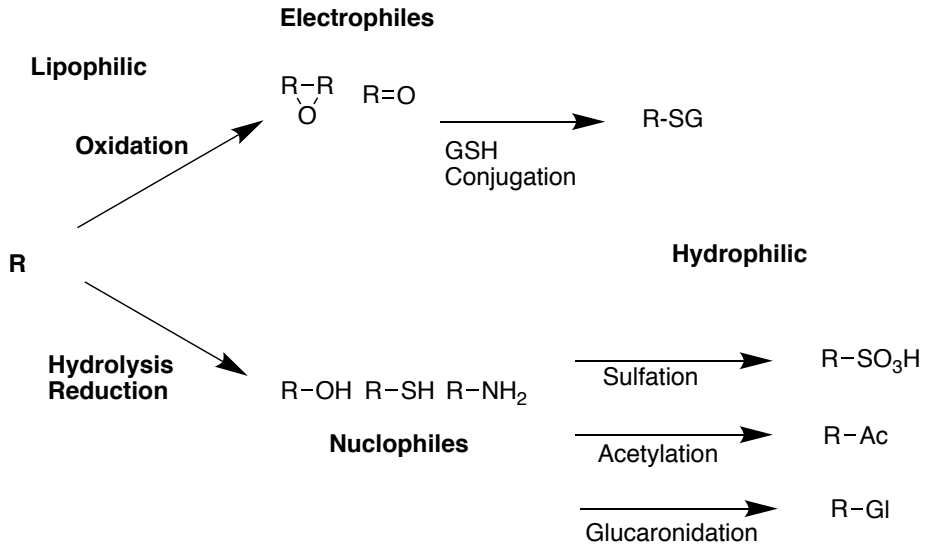

Figure 1.3: Phase I and phase II drug metabolism

Drug metabolic pathways can broadly be categorized as oxidative or reductive, or covalent modifications to the parent compound such as in phase 2 metabolism. Pathways shown display various detoxifying agents present in both phase 1 and phase 2 metabolism and the various known metabolic products of each phase. Phase I metabolic products tend to be electrophilic species produced by oxidation, reduction or hydrolysis of the parent compound. Phase II products tend to involve conjugation of certain molecules to the parent compound or metabolite to facilitate its removal. When certain detoxification pathways are depleted or not adequate, these metabolites persist in the body leading to various outcomes.

1.6 N-(4-HYDROXYPHENYL)ACETAMIDE

APAP is a commonly used analgesic and antipyretic. It can be used as a single-component medication, as well as in combination with other medications such as anti-histamines and ephedrine. (Temple et. Al, 2007). Best known for its marketing in the United Sates as Tylenol ®, APAP was introduced in 1955 as a prescription medication. Five years after its introduction, it became available as an over-the-counter (OTC) medication (Leon, 1983).

Overdose cases are common with APAP due to its widespread availability, resulting in 50,000 emergency room visits and 25,000 hospitalizations occurring annually in the United Sates

(Nourjah et al., 2006). APAP is also one of the major leading causes of ALF in the United States (David Josephy, 2005). The toxicity of APAP can stem from a major overdose event or repeated excessive dosing (Bond et al., 1999). Due to the large incidence of APAP induced hepatotoxic events, there are on-going research efforts to understand mechanisms of APAP hepatotoxicity (Bromer and Black, 2003).

APAP is absorbed by the gastrointestinal tract (GI) with peak concentrations at 90 minutes post therapeutic dosage, and a half-life of approximately 2.5h. In the presence of hepatic injury, the half-life of APAP is extended to approximately 4-5h (Prescott et al., 1971). APAP is rapidly and uniformly distributed within the tissues (Brodie, 1949). APAP undergoes extensive hepatic metabolism, where 85% of the therapeutic dosage undergoes phase II metabolism giving sulfated and glucuronidated products. These glucuronidated and sulfated metabolites are then renally excreted (Prescott, 1980). Approximately 10% of the therapeutic dosage undergoes phase I metabolism leading to the known toxic metabolite of APAP, N-acetyl-para-benzoquinone imine (NAPQI) (Gelotte et al., 2007).

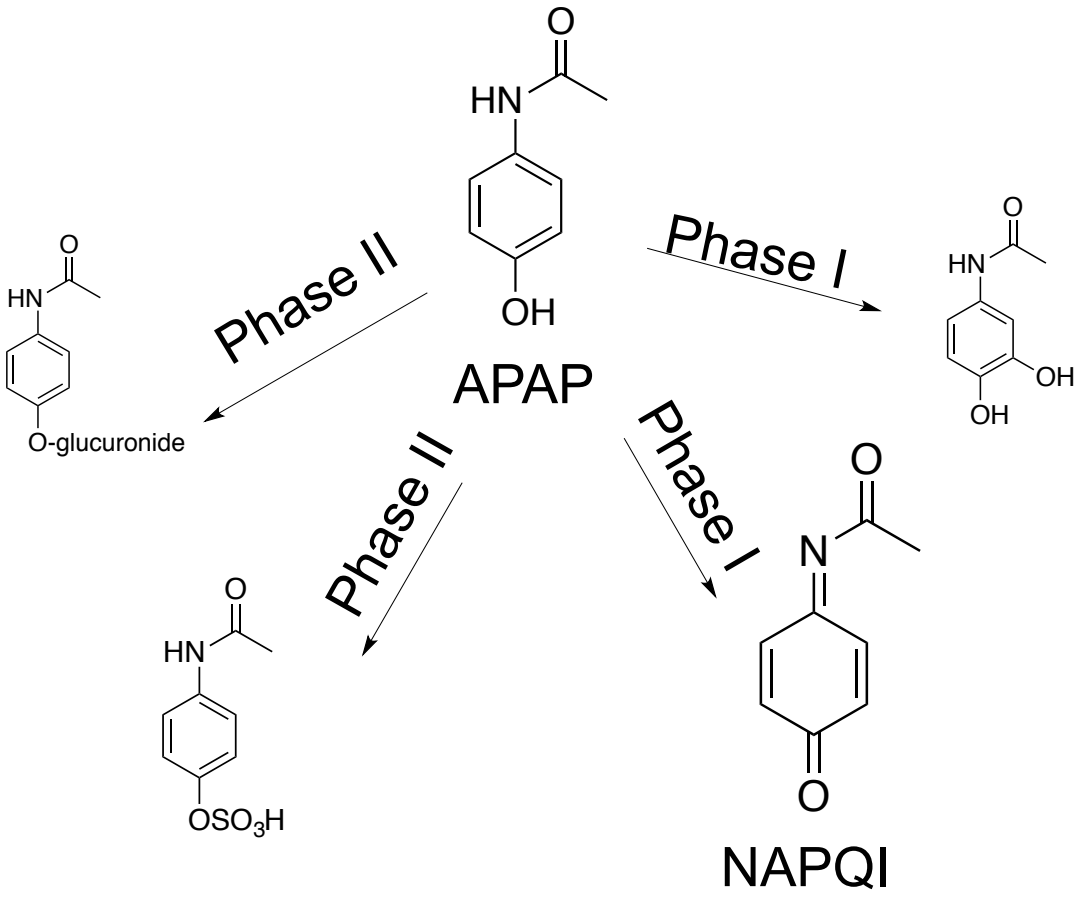

Figure 1.4: Phase I and phase II metabolism of APAP.
APAP undergoes both Phase I and Phase II metabolism. The Phase I metabolic product NAPQI is hypothesized to cause the hepatotoxic effects of the drug. Approximately 10% of a dosage is converted to NAPQI via cytochrome P450 oxidation. The remaining APAP can be sulfated and glucuronidated under Phase II metabolism in order to facilitate removal of the compound from the body.

1.8 Mechanism of Action of APAP

Although APAP is one of the most commonly used analgesics, its mechanism of actions is still not properly understood. APAP is often compared to non-steroidal anti-inflammatory drugs (NSAID) for displaying similar analgesic properties, although APAP does not display the same mechanism of action as the NSAIDs, namely the inhibition of cyclooxygenase enzymes COX-1 and COX-2

(Ouellet & Percival, 2001). It was proposed that there may be another distinct form of the cyclooxygenase enzymes, COX-3, which is expressed as a spliced variant of the COX-1 gene (Chandrasekharan et al., 2002). This COX-3 mechanism was inconclusive since the COX-3 variant was not found in humans after cloning studies. After extensive studies it is believed that APAP derives its analgesic and antipyretic properties from a mechanism of action different from the NSAIDS, which is still unknown (Davies, Good, Roupe, & Yáñez, 2004).

1.9 TOXICOLOGY OF APAP:

Approximately 10% of APAP undergoes phase I oxidation to the reactive quinonimine intermediate NAPQI (Bromer & Black, 2003). At non-toxic doses, NAPQI is conjugated with glutathione and forms nontoxic cysteine and mecapturate conjugates, preventing it from reacting with cellular proteins. Once the glutathione stores have been depleted NAPQI reacts with endogenous cellular proteins leading to cell injury or death (Mitchell, Jollow, Potter, Gillette, & Brodie, 1973). Most researchers agree that hepatic GSH depletion is the critical trigger for acetaminophen hepatotoxicity (Bessems and Vermeulen, 2001). Hepatocellular damage likely results from the aggregated effect of damage to multiple proteins and simultaneous inhibition of many enzymes and cellular functions (James et al., 2003). Mitochondrial oxidative stress, generation of reactive oxygen and nitrogen species, activation of stress proteins and gene transcription mediators, and mobilization of the liver's innate immune system are all important factors in the hepatocellular damage that occurs from APAP overdose (Leeming, Gamon, Wille, Donald, & O'Hair, 2015a). Increased concentrations of NAPQI lead to enhanced glutathione depletion, protein adduct formation and oxidation, and oxidative/nitrosative stress resulting in hepatocellular injury. APAP is probably the best characterised hepatotoxin in pre-clinical models, and therefore provides a means to interrogate the various processes of adaptation and

regeneration in the liver, which are also relevant to human and may be applicable to other drugs associated with DILI (Bromer & Black, 2003).

1.10 Regioselectivity of Thiol Arylation of NAPQI:

Thiol arylation of NAPQI has been investigated heavily using LC/MS and NMR experiments. Hinson et al. 1983, determined that 3-(glutathione-s-yl)acetaminophen was the major product of the reaction between NAPQI and GSH. The *ortho* hydroxyl regioselectivity was determined by intensively comparing the chemical shifts between APAP and GSH bound APAP. ^{13}C NMR was used to determine amido and hydroxyl aromatic carbons, and the thioether bound aromatic carbon was deduced due to a lower chemical shift. The upfield position of the aromatic carbon bearing the GSH adduct compared to other aromatic thioethers suggested that this change in chemical shift was indicative of an *ortho*-hydroxyl substituent. Upon analysis of the aromatic region it was evident that this was a 1,2,4-trisubstituted system with couplings of 2 and 8.5 Hz. 3-(glutathione-s-yl) acetaminophen was treated with sodium deuteroxide (NaOD) in order to validate the substitution of the aromatic ring. The NMR spectra with and without NaOD were compared and it was shown that only one aromatic proton displayed a change in chemical shift after treatment with NaOD (figure 5.1). The doublet at 6.78 ppm J=8.5 Hz moved upstream by approximately 0.3 ppm, indicating that this was the proton ortho to the phenolic group, supporting that the sulfur group was present at the C^3 site. Due to the data presented by Hinson et al., and further proof of these studies in the literature, binding of NAPQI to endogenous nucleophiles will be shown with the (3-s-yl)acetamoniophen as the major product.

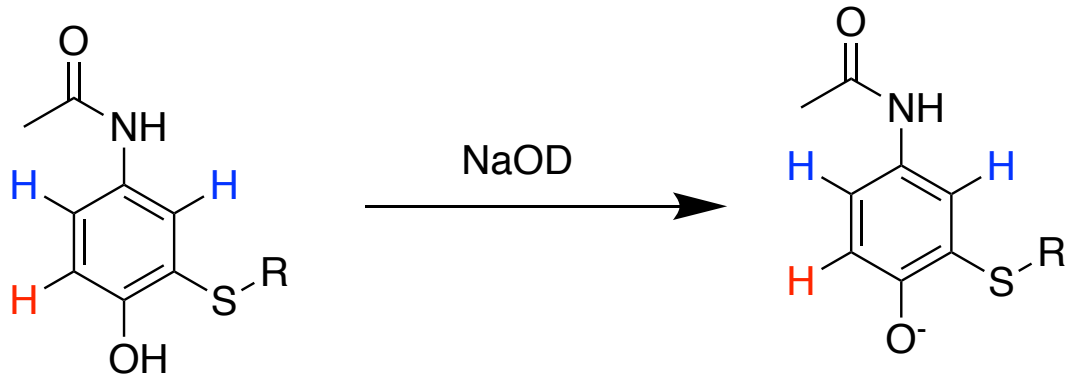

Figure 5.1:NMR Validation of thiol NAPQI regioselectivity

Hinson and colleagues performed several NMR experiments to validate the regioselectivity of NAPQI to thiol nucleophiles. NAPQI bound to a thiol nucleophile (GSH and Cysteine) was isolated. Addition of NaOD to the isolated product displayed a change in chemical shift to the ortho hydroxy proton (red) but the meta protons did not display a change in chemical shift. The addition of NaOD changes the electronic properties of the hydroxyl creating a larger negative charge on the oxygen, ultimately changing the electronics of the aromatic ring. This change in electronics would only change the chemical shift for the proton ortho to the hydroxyl.

1.11 Magnetic Resonance Imaging

Magnetic Resonance Imaging (MRI) is a form of non-invasive imaging used in biomedical imaging and clinical diagnostics. It is particularly useful due to its high spatial and temporal resolution and non-radiative properties. MRI generates contrast by using external magnetic fields to manipulate the nuclear spins of water. Superparamagnetic Iron oxide nanoparticles (SPION) are T_2-weight MRI contrast agents. T_2 contrast agent usually causes a darkening effect when observed in an MRI scan. This darkening, or decrease in signal is caused by the shortening of the T_2 relaxation time caused by the interaction of the SPION with the water proton. The decrease in

signal can be quantified and is proportional to the amount of iron, or SPION present in the tissue (Conde et al., 2014). The benefits of using SPIONs is that they are superparamagnetic, have low toxicity *in vivo*, and are readily commercially available. SPIONs are composed of inorganic iron oxide cores (γ-Fe_3O_4) and hydrophilic coating polymers such as poly ethylene glycol (PEG) and polysaccharides, in this case carboxy methyl dextran (CMX). These coatings are necessary as the inorganic core tends to aggregate and precipitate *in vivo* (Arami, Khandhar, Liggitt, & Krishnan, 2015). An added benefit of using CMX coated IONPs is the ability to couple peptides to their surface using simple water-soluble coupling methods described in this work.

2.0 Objectives:

2.1 Approach:

We propose to develop a magnetic nanoprobe bearing biomimetic nucleophilic sites that can selectively bind to reactive electrophilic drug metabolites. These nanoprobes can be used *in vivo* either during drug screening when evaluating lead compounds prior to animal studies, and will allow characterization of the reactive metabolites of known hepatotoxic drugs (Dimasi, 2001). Due to the difficulty of isolating and analyzing these metabolites *in vivo*, this innovative nanoprobe design implements a facile method for their trapping *in situ* in the livers of live animals. This design aims to characterize these toxic metabolites and potentially improve the drug discovery process.

2.2 Design of NP

The proposed design of our nanoparticle includes the following design characteristics (Fig. 3):

1. Consists of a magnetite (γ-Fe_3O_4) core with a carboxymethyl-dextran (COO-) shell with an average size of 50nm.
2. A PEG-Galactose that serves as a hepatocyte targeting group.
3. A nucleophilic trap that has a terminal nucleophilic residue and that is a substrate for the tobacco etch virus (TEV) protease.
4. The peptide will have a brominated phenylalanine (FBr) to create a biased detection method via LC/MS analysis. This bias is created through the abundance of the bromine atom giving a characteristic M+2 peak.

Figure 2.1: Schematic Representation of Proposed Electrophile Trap.

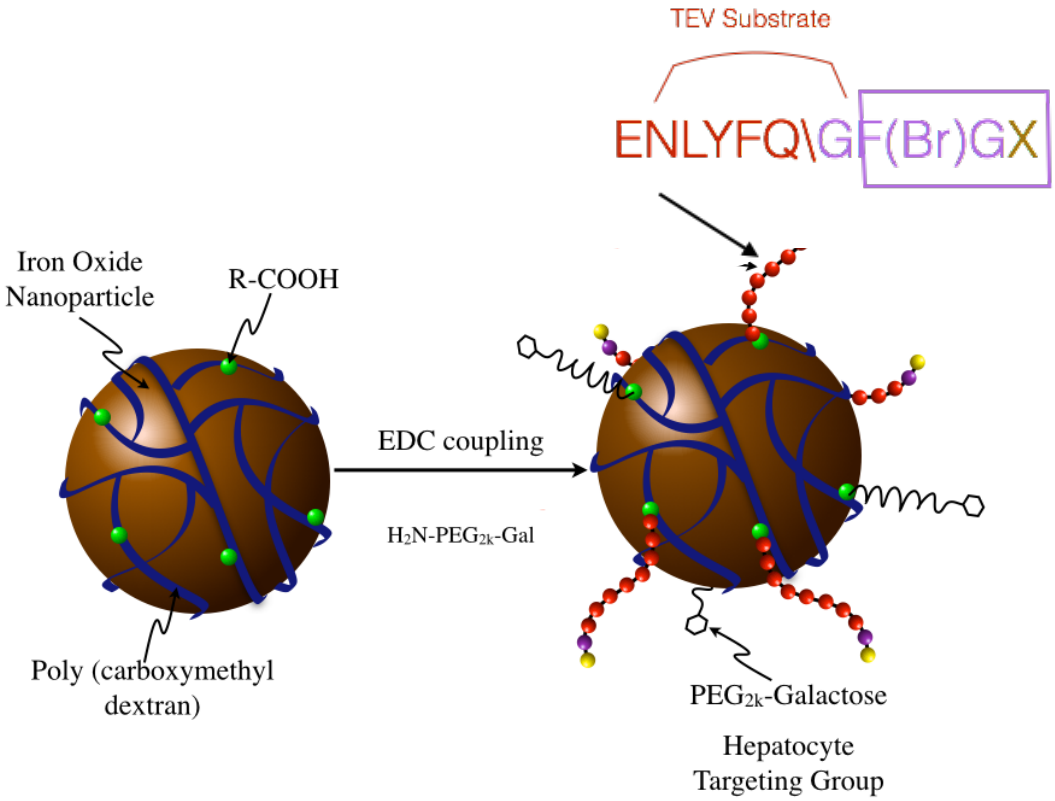

IONPs (Brown) are coated with carboxymethyl dextran (blue) bearing terminal functional carboxy groups (green). These carboxy groups will be used to couple two different functional groups. Bromine-containing peptides (red + purple) and hepatocyte targeting group (black) will be coupled to the IONP using 1-Ethyl-3-(3-dimethylaminopropyl)carbodiimide (EDC). Peptides will consist of various nucleophilic amino acids (yellow) which will bind to reactive metabolites. 3 different terminal amino acids will be explored: histidine, cysteine, and glycine (control). The TEV substrate (red) will be used to isolate and characterize the peptide bound metabolite. PEG=Polyethylene glycol, Gal = Galactose, TEV = Tobbaco etch virus.

The carboxy groups (COO-) will be coupled to a hepatocyte-targeting group (galactose moiety) (Hu, 2013) and a nucleophilic trap complex. The galactose moiety will allow the probe to be localized in the hepatocytes, which will be validated through T_2-weighted magnetic resonance imaging (MRI) (Tengowski, 2005). The electrophilic trap complex is composed of a peptide sequence that is substrate for the tobacco etch virus (TEV) protease (ENLYFQ|G sequence) (Phan,

2002). The TEV sequence will terminate in a nucleophilic amino acid (H, or C) bearing a terminal amide group to limit sites of drug reactivity (Srivastava, 2010). The phenylalanine (FBr) residue will have a *para*-substituted bromine. This FBr will create an isotope effect when carrying out MS analysis, since the presence of the bromine will create an M+2 peak that will facilitate specific detection relative to other peptide fragments recovered from the liver. Due to the superparamagnetic properties of the magnetite core the nanoparticle can be tracked using T_2-weighted MRI, and can be isolated via magnetic column separation.

2.3 HYPOTHESIS

We hypothesize that *intravenously* injected NP will covalently complex electrophilic drug metabolites *in situ* in the livers of live mice. The NP-metabolite complex will be recovered through extraction of the liver, and harvesting from homogenized liver tissue using magnetic column separation. Once the NP-metabolite complex is recovered, the terminal four amino acids covalently modified by the reactive drug metabolite will be isolated from the nucleophilic peptide *via* TEV protease processing directly off of the NP. Modifications to the parent compound can be analyzed and the metabolic pathways can be inferred by the metabolite detected. The well-characterized drug acetaminophen will be used to validate the method (McGill, 2013). With this information, structure-toxicity relationships can be validated, and drug safety may be improved.

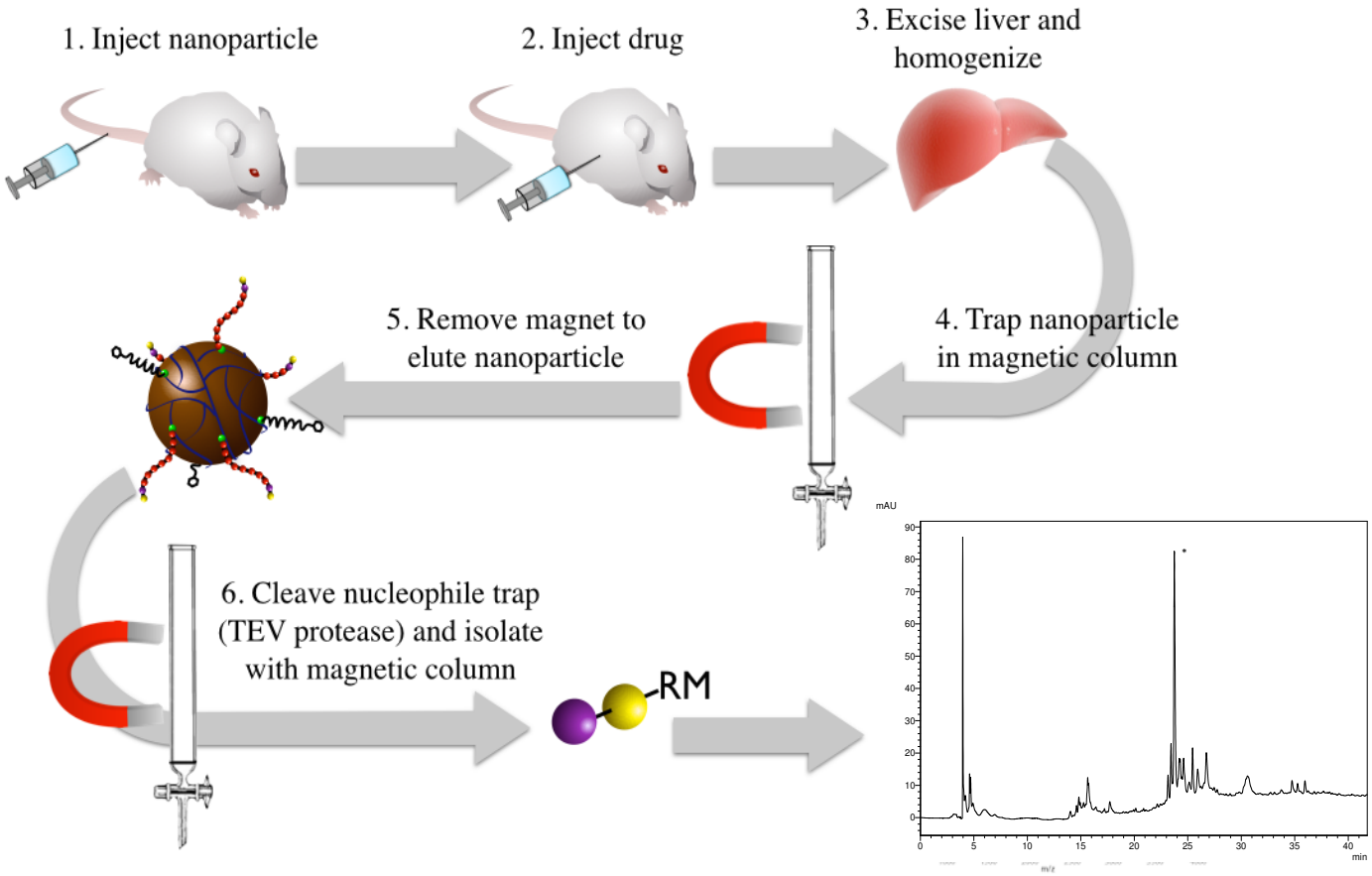

Figure 2.2: Methodology for Isolation of IONP from the liver of BALB /C mice and Characterization of Metabolite.

BALB/C mice were treated with IONP and drug for a certain period of time. The liver was extracted from euthanized mice and frozen. The frozen liver was homogenized and passed through a magnetic column allowing the isolation of the magnetic IONPs. Isolated IONPs were washed and treated with TEV protease in order to isolate the remaining peptide fragment. Recovered peptide-bound metabolite was analyzed using LC/MS analysis in order to identify the recovered compound.

2.4 Summary of Goals and Objectives:

As described above, the goal of our work is to design and implement a method for characterizing reactive metabolites in living organisms using the following method:

1. Synthesize and design a superparamagnetic IONP that can be injected into live mice, which will be functionalized using a peptide sequence and a hepatocyte targeting group. This peptide sequence will have a terminal nucleophilic species which will be able to react with electrophilic drug metabolites. This IONP will be monitored *in vivo* using T_2-weighted MRI to evaluate localization in the liver.
2. Design a method to extract this IONP *ex vivo* from the liver of mice using commercially available magnetic separation technology (Miltenyi Biotech). Separation will be facilitated by the superparamagnetic properties of the IONP, and will allow isolation of IONP from other liver components.
3. Implement this novel drug metabolite assay using APAP compound for method development due to its well-known toxic metabolite NAPQI. We can then potentially develop this method for the characterization of toxic metabolites of other drugs or drug candidates *in vivo*.

CHAPTER 3: MATERIALS AND METHODS

3.0 MATERIALS AND METHODS

3.1 SYNTHESIS OF NAPQI

N-Acetyl-Benzyl-Quinone-Imine was synthesized as follows:

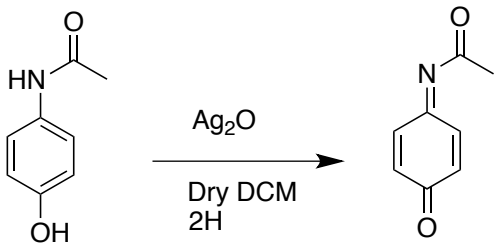

Scheme 3.1: The synthesis of NAPQI

Starting material APAP (3.3mmol) was suspended in dry DCM. To this mixture was added excess Ag_2O (6.4mmol) and the reaction was allowed to stir for 2h (Leeming, Gamon, Wille, Donald, & O'Hair, 2015b). The reaction was monitored via TLC (diethyl ether). The crude reaction mixture was filtered and subjected to silica gel chromatography using diethyl ether as the mobile phase. The crude reaction mixture was concentrated and then 10 mL of dry acetonitrile was added. The remaining diethyl ether was removed *in vacuo* and this NAPQI solution in acetonitrile was used for all subsequent experiments.

N-Acetyl-Benzyl-Quinone-Imine (NAPQI) was synthesized using the starting material APAP (Fisher Scientific) and Silver (I) Oxide (Sigma Aldrich, purchased commercially). APAP (0.50g, 3.30mmol) was suspended in 35 mL of dry DCM. Ag_2O powder (1.12g) was added to the suspended mixture and allowed to react for 2h monitored by TLC on silica solid phase with diethyl ether where an rf value of approximately 0.8 corresponded to NAPQI.

Ag_2O was filtered off once the reaction was complete, and the solution was subjected to silica gel chromatography with diethyl ether as mobile phase. NAPQI was isolated as a solid yellow eluant. All fractions were collected and combined, and diluted with 10 mL acetonitrile as NAPQI is

unstable in diethyl ether but is stable for less than 24 hours in acetonitrile. The diethyl ether was removed *in vacuo* and the remaining solution in acetonitrile was used for subsequent studies.

3.2 Glutathione Assay

L-Glutathione (GSH, 10 mg) (Fisher scientific) was dissolved in 0.1 mL 1.0× phosphate buffered saline (PBS) pH = 7.2. GSH was reduced using 0.1 equivalents tris(2-carboxyethyl)phosphine hydrochloride (TCEP) for 1h in order to remove any oxidized GSH and free the thiol nucleophile. The reduced GSH solution was incubated with 10 μL of the previously described NAPQI solution (3.2) for 3h with pH being monitored by pH paper and set to 7.0 with $NaHCO_3$. 100 μL aliquots of the reaction mixture were taken and diluted to 1mL and subjected to HPLC analysis with free GSH being the reference standard. The entire reaction mixture was collected using method A in HPLC protocols (3.1) and subjected to ESIMS characterization (3.2).

3.3 Peptide Synthesis

All peptide synthesis was carried out using solid phase peptide synthesis (SPPS) on the CEM liberty blue peptide synthesizer (CEM, United Kingdom). Synthesis was carried out using the Rink Amide resin (Chem Impex, United States) to give C-terminal amide peptides. Table 1.0 described the solutions and chemicals used and their role in SPPS. The following amino acids were used in the synthesis of 3 peptides, each bearing a different terminal amino acid residue. All amino acids were purchased from GL Biochem (China).

Table 3.1: List of all amino acids used and their respective protective groups.

All amino acids were coupled using fmoc solid phase peptide synthesis and had varying protecting groups depending on reactivity of R groups. All protecting groups were removed using trifluoroacetic acid:TIPS:DCM 95%:2.5%:2.5%. Terminal residue FMOC protecting groups were removed for coupling to nanoparticles using a 2.0M solution of methylamine in THF, and deprotection was validated using a ninhydrin stain.

Amino Acid	**Protecting Group(s)**
Glycine (G)	Fmoc
Glutamic Acid (E)	Fmoc, tBu
Asparagine (N)	Fmoc, tBu
Leucine (L)	Fmoc
Tyrosine (Y)	Fmoc
Phenylalanine (F)	Fmoc
Glutamine (N)	Fmoc, tBu
Histine (H)	Fmoc, Boc
Cysteine (C)	Fmoc, tBu

Table 3.2: List of solvents for SPPS and their roles in synthesis.

Each solution was prepared separately from the automated system. Protocols for preparation of these solutions was adopted from the Liberty Blue SPPS manual. Varations in the standard protocol include the use of the Rink Amide Resin, the use of 20% pyperizine instead of morpholine, and the use of HBTU alone as the activator solution.

Role	Chemical
Resin	Rink Amide Resin (0.25 mmol)
Deprotect	20% Pyperizine in DMF
Activator Solution	10% HBTU in DMF
Activator Base	35% *N*,*N*-Diisopropylethylamine and 65% N-Methyl-Morpholine
Main Wash	N,N-Dimethylformamide
Secondary Wash	Dichloromethane
Capping	Acetate

Rink amide resin (substitution 0.43 meq/g, 0.25 mmol) was dissolved in DCM and allowed to swell for 30 minutes. The resin was then placed in a reaction vessel and attached to the peptide synthesizer for subsequent reactions. The first step in SPPS is to deprotect the fluorenylmethyloxycarbonyl chloride (FMOC) bearing resin in order to allow subsequent couplings to occur. Amino acids (0.25 mmol) were dissolved in 6 mL of DMF, water bath sonication was used to successfully dissolve more hydrophobic amino acids. Completely dissolved amino acid solutions were then attached to the peptide synthesizer under their respective three letter codes. Peptide synthesis proceeded overnight, and coupling was verified using software

based substitution calculations. A substitution factor of 2.0 or higher was sufficient for proceeding with the following coupling. Once all amino acids were successfully coupled, the resin was returned from microwave into reaction vessel, and completed peptides were washed thoroughly 10 times with DMF and 10 times with DCM. After final wash with DCM peptide loaded resins were stored at -20°C.

Table 3.3: Yield and sequencing of peptides

Each sequence has a given name derived from their chemical synthesis (R = rink amide) (resin), the middle letter signifies the terminal nucleophilic residue and P denotes peptide. Each sequence has a modified phenylalanine residue with a bromine attached at the para position, and their respective yields are cited. Some peptides have lower yields due to the presence of impurities and reduced retention of the sequence from the resin. Peptides were synthesized at a 2 mmol scale initially but were scaled up upon successful synthesis and as needed.

Name	Sequence	Yield
RCP	ENLYFQGF(Br)GC	65%
RHP	ENLYFQGF(Br)GH	50%
RGP	ENLYFQGF(Br)GG	68%
RCPF	GF(Br)GC	65%

3.4 Cleavage and Isolation of Peptides

Peptides on resin were removed from the synthesizer and placed in a filtered reaction vessel for subsequent experiments. Resin was washed 10x with DMF and 10x with DCM and dried using pressured air. Once adequately dried, a solution of 95%TFA:2.5%DCM:2.5% triisopropylsilane (TIPS) was prepared for deprotection of remaining protective groups and cleavage of the peptide from the resin. Peptides were incubated with the solution for approximately 2-3 h and shaken at room temperature using a bench top shaker. Histidine peptides were incubated for longer periods

of time (4-5h) to ensure better recovery of the peptide. Solvent was removed by applying pressurized air and outflow solution was monitored by TLC plates illuminated by UV lamp. Peptides were dried *in vacuo* and precipitated in diethyl ether. Peptides were isolated using centrifugation at 4000RPM for 4 minutes, supernatant was disposed of and remaining pellet was used for subsequent experiments. In some cases the supernatant of the peptide solution was coloured and in this case it was not disposed of but subsequent precipitations were carried out until the supernatant was clear. The pellet was dissolved in water and purified via HPLC and lyophilized to a dry powder (section 3.10). In all cases peptides were isolated and characterized with FMOC protecting group still present in order to limit the sites of reactivity of the peptides when performing subsequent *in vitro* experiments. FMOC deprotection was carried out in order to couple the N-terminus with IONP in quantitative yield using a 2.0M solution of methylamine in THF (3h). Methylamine solution was removed *in vacuo* followed by 3x precipitation of deprotected peptide in cold diethyl ether, and deprotection was confirmed using ninhydrin stain.

3.5 NAPQI Assay with Peptides

Isolated and purified peptides were incubated with the previously described (3.3mM) NAPQI solution. Peptides were dissolved in 100μL 1.0× PBS pH = 7.2 similar to the protocol described in section 3.2. NAPQI solution (100 μL of 3.3mM) was added to this mixture and incubated for 3 hours at room temperature. 50 μL Aliquots of the reaction mixture were taken and subjected to analytical HPLC to monitor the completion of the reaction. HPLC traces were monitored for 3 hours until no changes in traces were noticed. All peaks collected were subjected to ESIMS to determine binding of peptides with NAPQI.

3.6 SYNTHESIS OF PEG-GALACTOSE TARGETING GROUP

A hepatocyte targeting group was synthesized using the following method (Scheme 3.1).

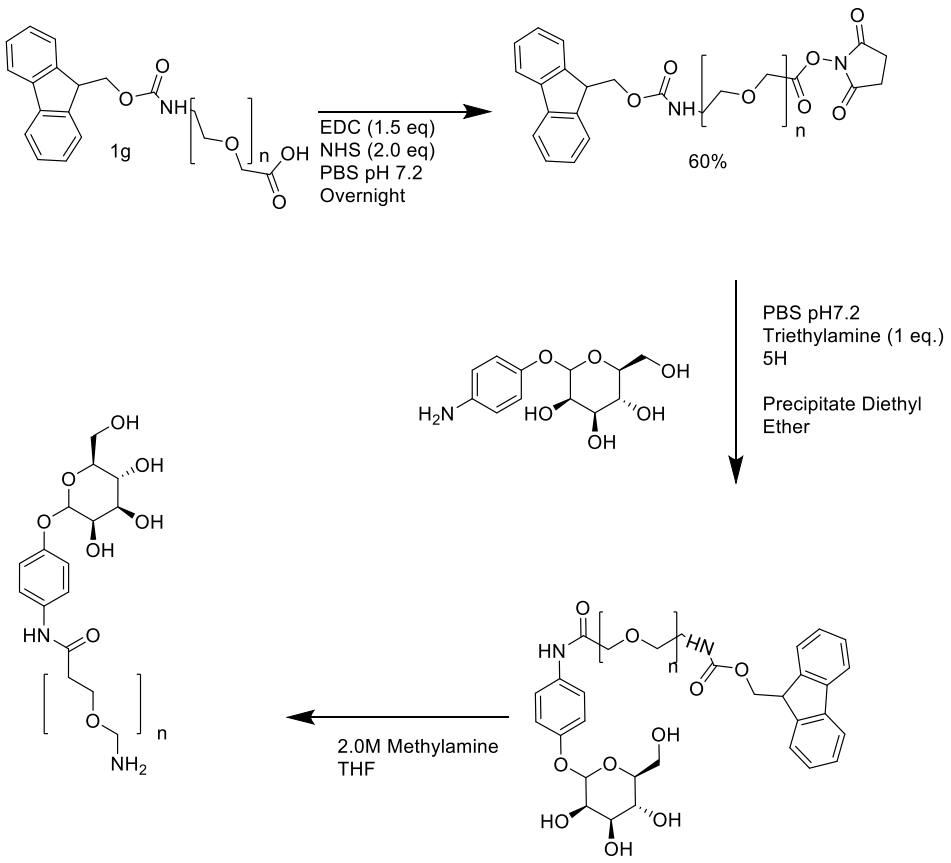

Scheme 3.2: Synthesis of galactose targeting group.

Fmoc-NH-(PEG)-COOH (2000 Da) was purchased and activated using EDC and NHS. To the activated NHS ester was added 4-Aminophenyl β-D-galactopyranoside. The reaction was allowed to stir overnight and was stopped using a diethyl ether precipitation. This mixture was spun down at 4000RPM for 2 minutes and the supernatant was discarded. This process was repeated 3 times and the pellet was dissolved in 2.0M methylamine in THF in order to deprotect the FMOC group. The resulting product was purified using HPLC.

Fmoc-NH-(PEG)-COOH (2000 Da) was purchased from JenKem Scientific and was activated overnight on ice using 1-Ethyl-3-(3-dimethylaminopropyl)carbodiimide (EDC) and N-hydroxysuccinimide (NHS) in PBS buffer at pH = 7.2. Activation of the compound was confirmed

via H^1 NMR (400Mhz, Bruker). Once activated, 4-Aminophenyl β-D-galactopyranoside was added and allowed to react overnight. Deprotection was carried out using 2.0M methylamine in THF. The reaction mixture was dried *in vacuo* and then precipitated in cold diethyl ether and centrifuged at 4000RPM for 4 minutes. The precipitate was HPLC purified using method B and subjected to NMR (400MHz, MeOD) characterization.

3.7 Conjugation of Peptides and Targeting Group to NP

Magnetite (γ-Fe_3O_4) NPs were purchased from Chemicell bearing a carboxy methyl dextran coating with a size of 50nm (CMX-IONP). NPs (0.75mg in 100μL of 1X PBS buffer) were activated with 1 mass eq. EDC and 1.5 mass eq. NHS for 3 hours similar to the protocol described in 3.6. Activated particles were washed with 1X PBS buffer using a size exclusion column (Amicon 25KDa) allowing all side products to be removed and resuspended in 100 μL of clean 1.0× PBS. The NP solution was transferred to a clean Eppendorf tube in 100 μL of 1.0× PBS and incubated overnight with 5mg of purified peptide and 1 mg of targeting group. Six different types of NPs were synthesized for subsequent studies, of which three were targeted and three were untargeted (Table 2.3).

Table 3.4: Synthesized IONPs and their properties.

Listed here are the different IONPs synthesized and their respective peptide sequence. Each IONP was synthesized in duplicates with and without the presence of targeting group. Each IONP category varied based on its terminal amino acid residue. Duplicates were made in order to investigate the effect of the targeting group and if its presence changed the retention of the IONPs in the liver.

Name	Peptide	Targeted (yes/no) (presence of Gal-PEG)
RCP-1	ENLYFQGFGC	Yes
RCP-2	ENLYFQGFGC	No

RHP-1	ENLYFQGFGH	Yes
RHP-2	ENLYFQGFGH	No
RGP-1	ENLYFQGFGG	Yes
RGP-2	ENLYFQGFGG	No

These NPs were then washed ten times using the Amicon MW 25K centrifugation filters and resuspended in 100 µL of 1.0× PBS, eluent was monitored until no UV activity was present. Clean NPs were transferred to sterile falcon tubes for use in subsequent experiments and suspended in 100 µL of 1.0× PBS to a final concentration of 0.75mg/100µL.

3.8 NAPQI Assay with NPs

Synthesized and washed NPs (section 3.7) (0.75mg/100µL) in 1.0× PBS were diluted in 500 µL pH = 7.2 1.0× PBS buffer. The mixture was vortexed and sonicated to ensure adequate suspension and that no aggregation was occurring. As described in section 3.1 a solution of NAPQI (3.3mM) was added to the suspended NPs and allowed to incubate over night at room temperature with agitation using a shaking bed. Varying amount of solution was added ranging from 10 µL to 200 µL. The reaction mixture was washed 4x with 1.0× PBS in order to remove any unreacted species. Washed NPs were stored at 4°C prior to subsequent experiments.

3.9 TEV Protease Assay

Washed and purified NPs (0.75mg/100µL) conjugated with peptide and targeting group were placed in an Eppendorf tube and incubated with 1 reactive unit or 2.0 µL of TEV protease (Sigma, Oakville Ontario) overnight at 37°C using a heating block. 50 µL Aliquots of the reaction mixture were taken before and after addition of protease, diluted to 1mL H_2O and subjected to HPLC analysis. Reaction mixture was separated using the same Amicon 50 000 Da filter preventing

IONPs from passing through. HPLC trace was monitored, peaks were collected and subjected to ESI MS to identify cleavage products.

3.10 HPLC PURIFICATION

High performance liquid chromatography (HPLC) was used to both characterize and purify all compounds. Purity tests and analytical runs were performed using method A whereas semi-preparative-scale purification were performed using method B. All runs were performed using water as phase A and acetonitrile as phase B. Analytical runs were performed to determine >95% purity of crude mixture by area under the curve (AUC) measurements, and to ensure purity of final product. Samples were also collected from analytical runs and characterized via MS (section 3.2). Method B was used to perform purification. Purification was performed using a 5-mL injection port and a flow rate of 10 mL/min. Samples purified using method B were lyophilized to a white powder then subjected to Method A for purity measurement. All peptides were deemed >95% pure.

Method A: Luna 5 μm C-18 100Å 250x4.6 mm column (Phenomenex, Torrance, United States) was eluted with gradient solvent system of phase A (water + 0.1% TFA) and phase B (acetonitrile + 0.1%TFA) at 1 mL/min. The elution profile is 99% phase A and 1% phase B initially to 1% phase A and 99% phase B over 45 min.

Method B: Luna 5um C-18 100Å 250x4.6 mm column (Phenomenex, Torrance, United States) was eluted with gradient solvent system of phase A (water + 0.1% TFA) and phase B (acetonitrile + 0.1%TFA) at 10 mL/min. The elution profile is 99% phase A and 1% phase B initially to 1% phase A and 99% phase B over 45 min.

3.11 Mass Spectrometry

Time of flight (TOF) Electrospray Ionization Mass Spectrometry (ESIMS) was used to characterize all compounds synthesized in these experiments. All samples that underwent TOF ESIMS characterization were done at the John L Holmes mass spectrometry facility (Ottawa, ON, Canada). All samples were stored in a mixture of acetonitrile (50%):water(50%): (0.1%)Trifluoro acetic acid (TFA) pH=3, and subjected to MS analysis in these solvent conditions. Only samples that underwent protease activity were stored in ammonium bicarbonate pH=8. The solvent system of the MS was acetonitrile:water and the nebulizing gas was nitrogen. Argon gas was used as the envelope gas system. Solvent spray was verified at a rate of 0.5 mL/min. Peptide peaks were characterized using CID characterization, and peptides bearing a bromine were identified using isotopic abundance and the presence of an M+2 peak.

3.12 MRI Imaging with IONPs

All animal work was approved by the University of Ottawa IACUC under AUP sc-2578. 100μL of 0.75 mg IONPS were thoroughly washed with sterile saline and then suspended in 100 μL of sterile saline. All imaging studies were done using MR solutions Preclinical MRI system at 3T at The University of Ottawa Heart Institute (Ottawa, ON, Canada). Female Balb/c mice were used for these studies. T_2-weighted Fast Spin Echo pulse sequence was employed with the following parameters:

Table 3.5: Parameters of T2-weighted (COR) MRI scans.
MRI parameters used in to monitor IONPs *in vivo*. Scans were conducted at 3T field strength in BALB/C mice.

Parameter	Value
Slices	10
Field of View (FOV)	80.00
FOV Ratio	0.50
TE	64 ms
TR	4500 ms

Scans were acquired prior to NP injection and every 10 minutes for 90 minutes after injection. Three different NP formulations were tested: unmodified CMX-IONP, ENLYFQGF(Br)GG-modified NP, and ENLYFQGF(Br)GG + PEG-Gal modified NP. Each group contained 3 mice. NP (0.15 mg) were suspended in saline and injected intravenously (i.v.) via tail vein cannula set prior to scanning. Mice were anesthetized using 2% Isofluorane and injections were prepared through a 1-meter line leading out of the MRI system. Initially a 100 µL saline solution was injected into the mice to perform base line scans, followed by a 100 µL injection of the suspended NP solution.

3.13 Image Analysis

All image analysis was performed using Vivoquant ® (Boston, United States). Using Vivoquant liver ROIs were generated using a lower limit of 250 (units) and a maximum of 1000 (units). All outliers were removed manually using the integrated brush setting. Heat maps were generated using the NIH colour scheme, giving a clear indication of signal intensity. Images were divided in to three sections: unmodified NPs, untargeted NPs, and targeted NPs and will be described using

these respective names. 3 balb/c mice were tested in each of these sections giving a total of 9. In these images, a decrease in colour scheme intensity shows an increase in T_2 weighted MRI signal, hence after injection of the NP a decrease in colour intensity is observed correlated with an increase in T_2 signal intensity.

3.14 ROI Statistical Data

ROI raw data was derived using Vivoquant software with a lower limit of 250 units and an upper limit of 100 units. All outliers were removed manually to ensure only liver data was observed. T=0min was used as the baseline scan for all subjects, and signal change was measured as a percentage change compared to the baseline ROI value. Each plot was expressed as an average of two mice.

3.15 Magnetic Separation

Magnetic separation was used to isolate and purify NPs. A MACs stand was purchased with a built-in magnet and was used for all separation procedures (Miltenyi Biotech, Germany). Minimacs columns were placed inside the magnetic field to perform separation experiments as described in the vendor protocol. Initially the column was activated with 500 µL of 1.0× PBS pH=7.2 and allowed to run through. The sample was then applied to column and collected in a falcon tube. The applied sample was washed twice with 500 µL 1.0× PBS and eluent was set aside. The column was removed from magnetic field and 100 µL of 1.0× PBS was forced through using a plunger. Final elution outside of magnetic field contained magnetic NPs, if no recovery was observed successive elutions were performed, and NP elution and concentration was verified using absorbance spectrometry.

3.16 *Ex vivo* NP Isolation

Balb/C mice (n=5 per group) were fasted for 8 hours prior to treatment by intraperitoneal injection of either saline or 300mg/kg APAP. After 30 minutes, both treated and untreated mice were given a 100 μL injection of 0.75 mg/100μL of targeted cysteine coupled (RCP-1) NPs. 1-hour post NP injection the mice were euthanized and the livers were excised and frozen at -80°C.

Frozen livers were removed from -80°C freezer and placed in a falcon tube in dry ice. A mortar and pestle were obtained and cooled using liquid nitrogen to preserve a cold environment and to prevent tissue thawing. The liver was placed inside the mortar and pestle and crushed into a fine powder and until no chunks were visible. This powder was placed inside a new sterile falcon tube and placed on dry ice. A 10X solution of radioimmunoprecipitation assay (RIPA) lysis buffer was prepared, and 5-7 mL of buffer was placed in the falcon tube. This solution was then homogenized using a cell sonicator until the solution was completely homogenized. Homogenized solution was passed through a magnetic separation column with steel wool and all byproducts were allowed passed through the filter. The IONPs were thoroughly washed under the presence of the magnetic field until the eluent was clear. Once the IONPs were adequately washed they were eluted out of the column be removing the column from the magnetic field, demagnetizing the steel wool. Due to the large surface area of the steel wool several elutions were necessary in order to get recovery of IONPs. In some cases, no IONPs were recovered due to the low concentration of IONPs present in the liver. A 10x increase in injection concentration of IONPs from 0.75mg/kg to a 7.5 mg/kg in order to improve recovery of IONP and achieve an adequate lower limit of detection.

CHAPTER 4.0: RESULTS

4.1 GSH BINDING ASSAY

NAPQI was synthesized using Ag_2O oxidation and purified as a solution in acetonitrile following the method described (Leeming, Gamon, Wille, Donald, & O'Hair, 2015) (figure 4.1A). NAPQI reactivity and covalent capture was tested with GSH, the endogenous nucleophile used to covalently modify NAPQI for its detoxification (figure 4.1A). The reaction was characterized using HPLC and MS analysis (Figs. 4.1B and C). The HPLC displayed multiple peaks in the reaction mixture, but only the selected peak (*) was subjected to HPLC and MS analysis giving the M^+ peak of 456.1422AMU, correlating to the mass of glutathione bound to NAPQI. Although in the literature the major product is seen as the 3' substituted thiol conjugate, other products may be possible depending on the concentration of NAPQI and nucleophile (Leeming et al., 2015). MS was performed only on the collected peak in order to validate the presence of the GSH-NAPQI bound molecule. The proposed structure of the product can be seen in figure 4.1A. Although multiple peaks are present in the HPLC spectrum, only the peak denoted with a * (figure 4.1B) was collected and subjected to MS analysis. Since NAPQI is a very good Michael acceptor and strong electrophile, these peaks may also be cross reactions with TCEP, which was used as a method to reduce any oxidized. TCEP can undergo phospha-Michael addition which may be an impurity present in the reaction (Y. J. Lee, Kurra, & Liu, 2016).

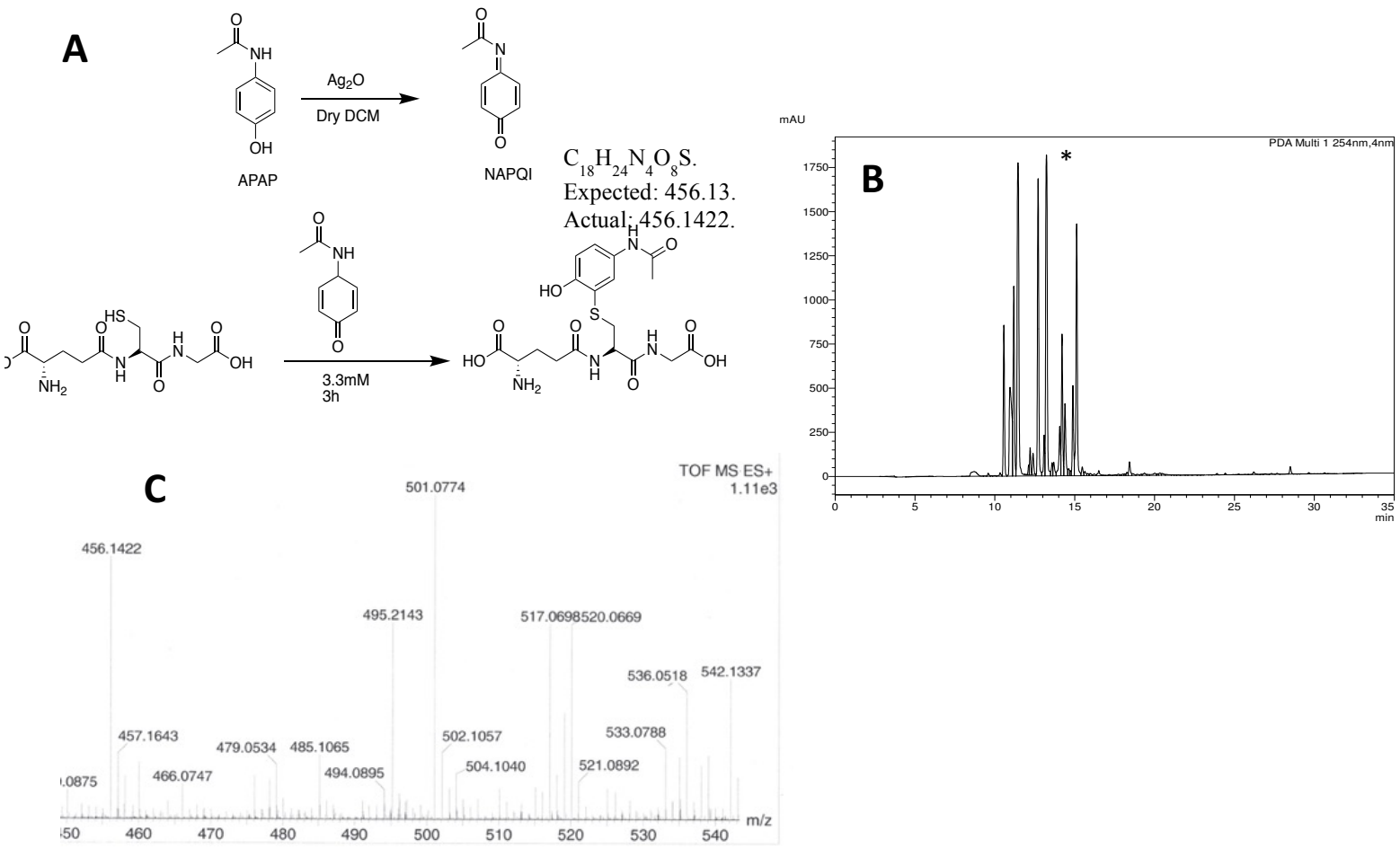

Figure 4.1: Characterization of GSH-NAPQI Adduct

A: 3mM of NAPQI was reacted with reduced glutathione to detect the presence of a GSH-NAPQI adduct. MF: $C_{18}H_{24}N_4O_8S$. Expected: 456.13. Actual: 456.1422.

B: HPLC spectra of the reaction between NAPQI and GSH showed the presence of multiple peaks. The GSH-NAPQI adduct was seen in the peak denoted with a * through collection of the peak and analysis via MS. HPLC spectra was completed using Method A at and analytical scale and flowrate of 1mL/min. No purity tests were performed.

C: The presence of the adduct was confirmed using MS where the M+=456.1422. This data supports the reaction of NAPQI with GSH.

4.2 Peptide Synthesis

3 peptides and one peptide fragment were synthesized by solid phase peptide synthesis (SPPS) using Rink amide resin at a scale of 0.2 mmol. Each peptide sequence varied based on the c-terminal amino acid residue. The peptide sequences synthesized were ENLYFQGF(Br)GX where X denotes the terminal residue cysteine, histidine, or glycine. These sequences were carefully chosen in order to test the reactivity of NAPQI, where the glycine peptide acted as our control due to the lack of a terminal nucleophilic residue. The peptide fragment synthesized was GF(Br)GC, which was expected to be cleaved from the peptide-bound iron oxide nanoparticle after treatment with TEV protease and thus acted as a standard compound. Purity traces and high resolution ESI MS (figure 4.2 to 4.4) were performed on all peptide sequences in order to validate structure and purity. For each peptide synthesized, the MS confirmed the identity of the product, and the purities ranged from 70% to 95%. Histidine peptide was shown to have a lower purity than the other peptide sequences due to a lower level of substitution to the resin (Meienhofer & Trzeciak, 1971). Peptides were characterized with FMOC protecting group still present in order to block the N-terminal and prevent reactivity with NAPQI for *in vitro* assays. FMOC protecting groups were removed prior to coupling to the NP using a 2.0M solution of methylamine in THF, leading to a quantitative deprotection. Peptide identity was also verified using the specific peak pairs of the sequence arising from the unique atomic abundance of Br, Br^{79} and Br^{81} (figure 4.2C). The Br^{79} peak can be identified in figure 4.2C as the M^{+}= 1498.5066AMU peak and the Br^{81} peak can be identified as the M^{+}=1500.5012 peak. This type of MS characterization was performed on all synthesized peptides. The synthesized fragment was designed to confirm the presence of our

peptide in HPLC experiments after treatment with TEV protease. The fragment is the chemical structure of our peptide sequence after treatment with TEV protease.

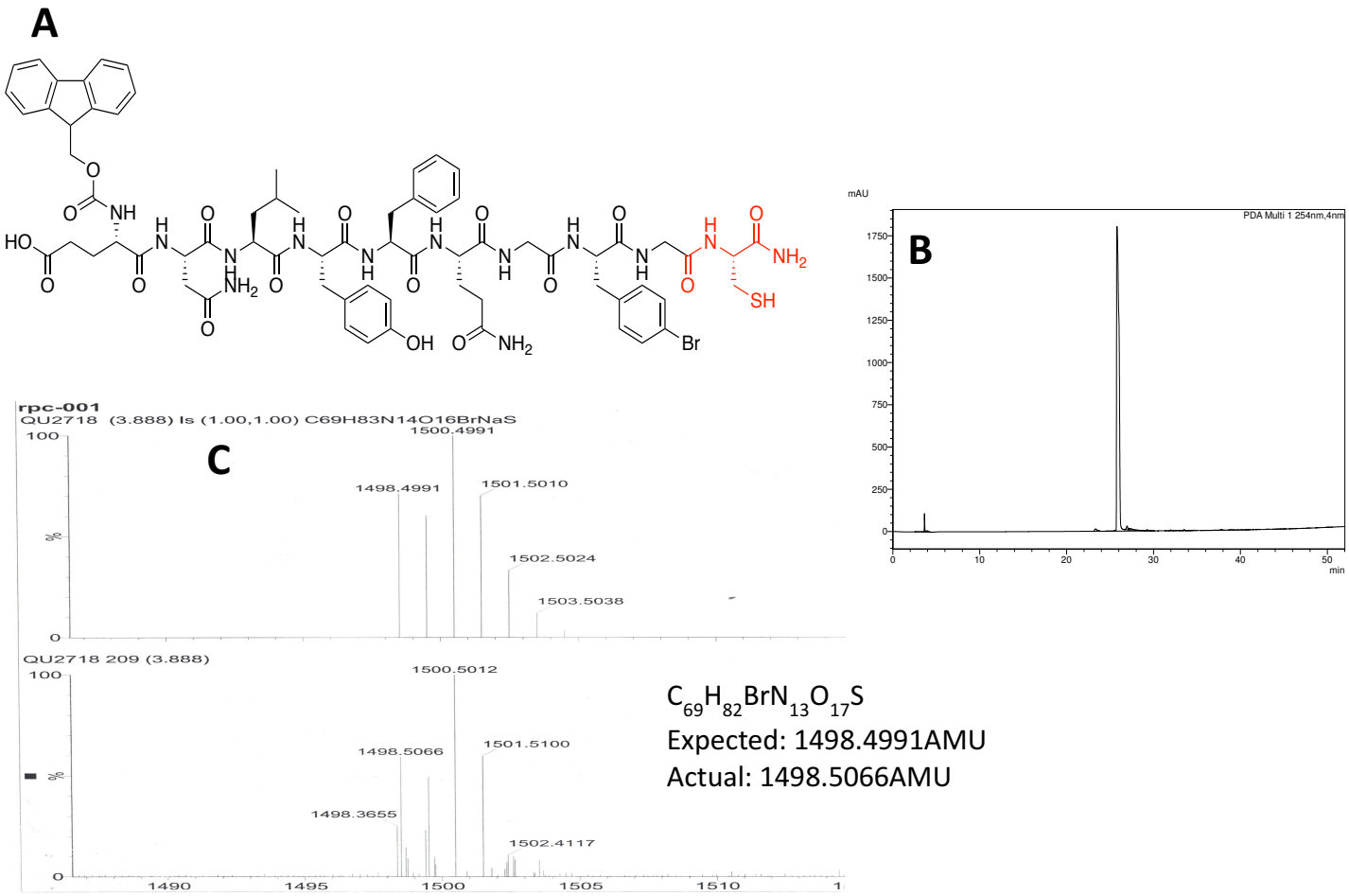

Figure 4.2: Structure and Characterization of ENLYFQGFGC (RCP) peptide.

A: The terminal residue is a cysteine nucleophile (red) and our isotopically labelled phenylalanine residue can be seen with a bromine at the *para* position. The atomic abundance of bromine is used here as a method to identify our peptide when performing MS experiments. The c-terminal of this peptide has been modified to an amide.

B: ***Analytical HPLC trace of RCP peptide***.

Conducted using method A at a flow rate of 1mL/min at concentraion of 1mg/mL. The major product is denoted with a *. The product was characterized using ESI MS, and and peak before 10 minutes denotes a solvent peak. The product was calculated as >95% pure. Purification on this peptide was performed using method B semi prep HPLC. All purity tests were done at 254 nm and all impurities were accounted for.

C: MS characterization of cysteine peptide sequence

ESI MS analysis was performed on the purified product, and the identity of this peptide sequence was verified with a M+ mass of 1500.5012. Some of the product remained in a M^+ state where as the other attained a Na^+ ion giving us

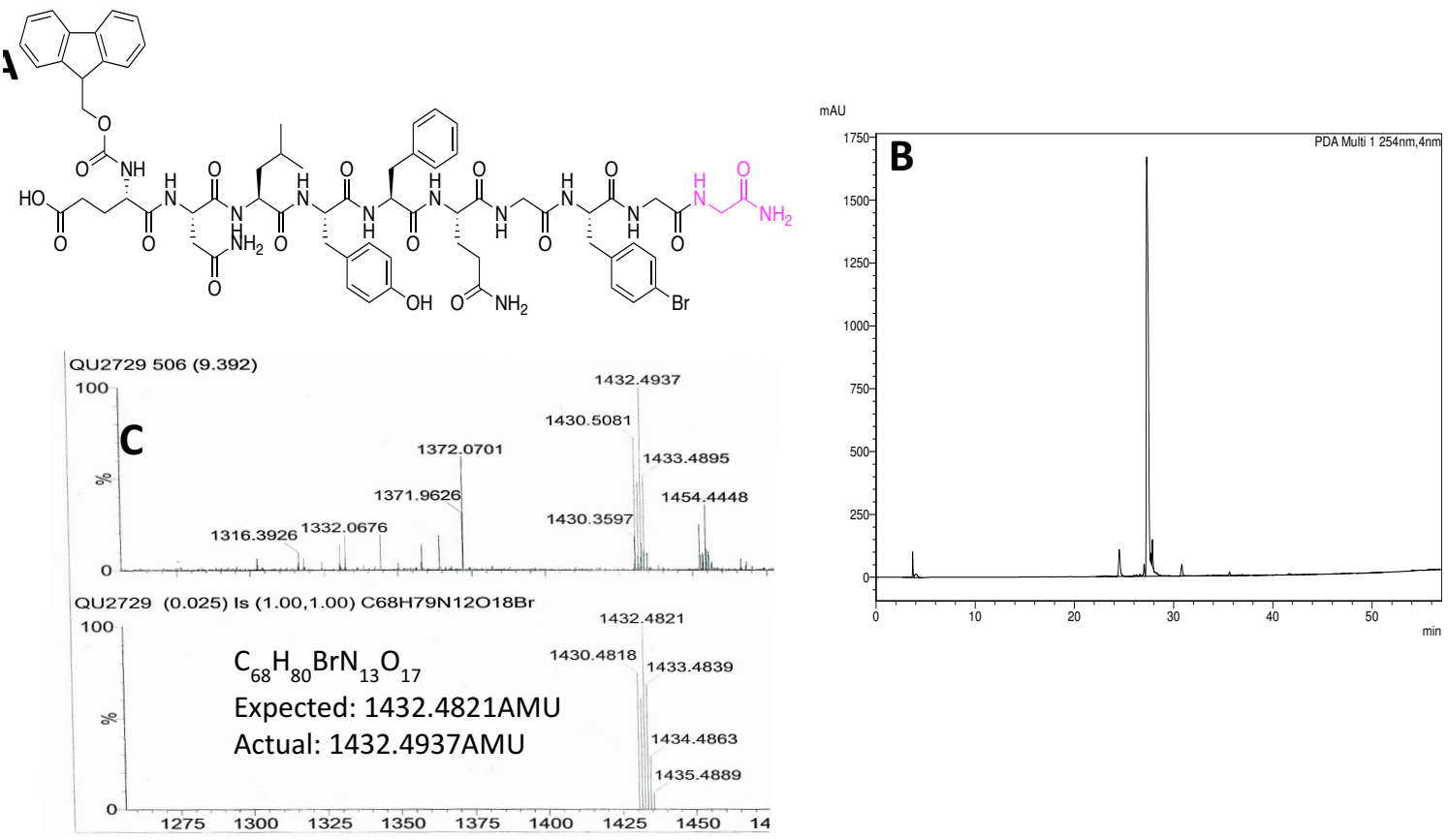

Figure 4.3: Structure and Characterization of ENLYFQGFGG (RGP) peptide.

A: The terminal residue is a glycine residue (pink) and our isotopically labelled phenylalanine residue can be seen with a bromine at the *para* position. The atomic abundance of bromine is used here as a method to identify our peptide when performing MS experiments. The c-terminal of this peptide has been modified to an amide.

B: ***Analytical HPLC trace of RCP peptide***.

Conducted using method A at a flow rate of 1mL/min at concentraion of 1mg/mL. The major product is denoted with a *. The product was characterized using ESI MS, and and peak before 10 minutes denotes a solvent peak. The product was calculated as <95% pure. Purification on this peptide was performed using method B semi prep HPLC. All purity tests were done at 254 nm and all impurities were accounted for.

C: MS characterization of cysteine peptide sequence

ESI MS analysis was performed on the purified product, and the identity of this peptide sequence was verified with a M+ mass of 1432.4821. Some of the product remained in a M^+ state where as the other attained a Na^+ ion giving us the MNa^+ Peak.

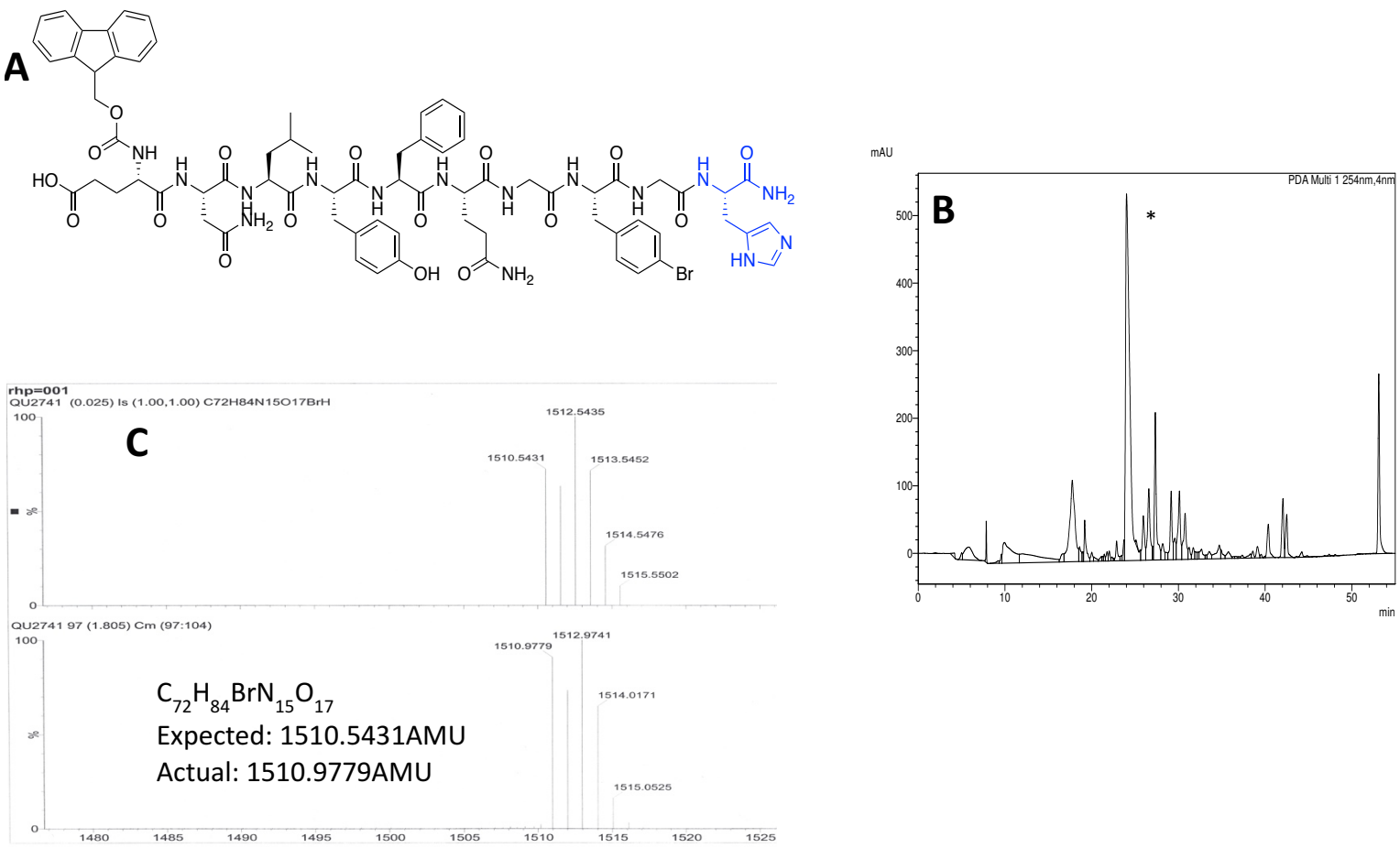

Figure 4.4: Structure and Characterization of ENLYFQGFGH (RHP) peptide.

A: The terminal residue is a histidine nucleophile (blue) and our isotopically labelled phenylalanine residue can be seen with a bromine at the *para* position. The atomic abundance of bromine is used here as a method to identify our peptide when performing MS experiments. The c-terminal of this peptide has been modified to an amide.

B: ***Analytical HPLC trace of RCP peptide***.

Conducted using method A at a flow rate of 1mL/min at concentraion of 1mg/mL. The major product is denoted with a *. The product was characterized using ESI MS, and and peak before 10 minutes denotes a solvent peak. The product was calculated as <95% pure. Purification on this peptide was performed using method B semi prep HPLC. All purity tests were done at 254 nm and all impurities were accounted for.

C: MS characterization of cysteine peptide sequence

ESI MS analysis was performed on the purified product, and the identity of this peptide sequence was verified with a M+ mass of 1512.9741. Some of the product remained in a M^+ state where as the other attained a Na^+ ion giving us the MNa^+ Peak

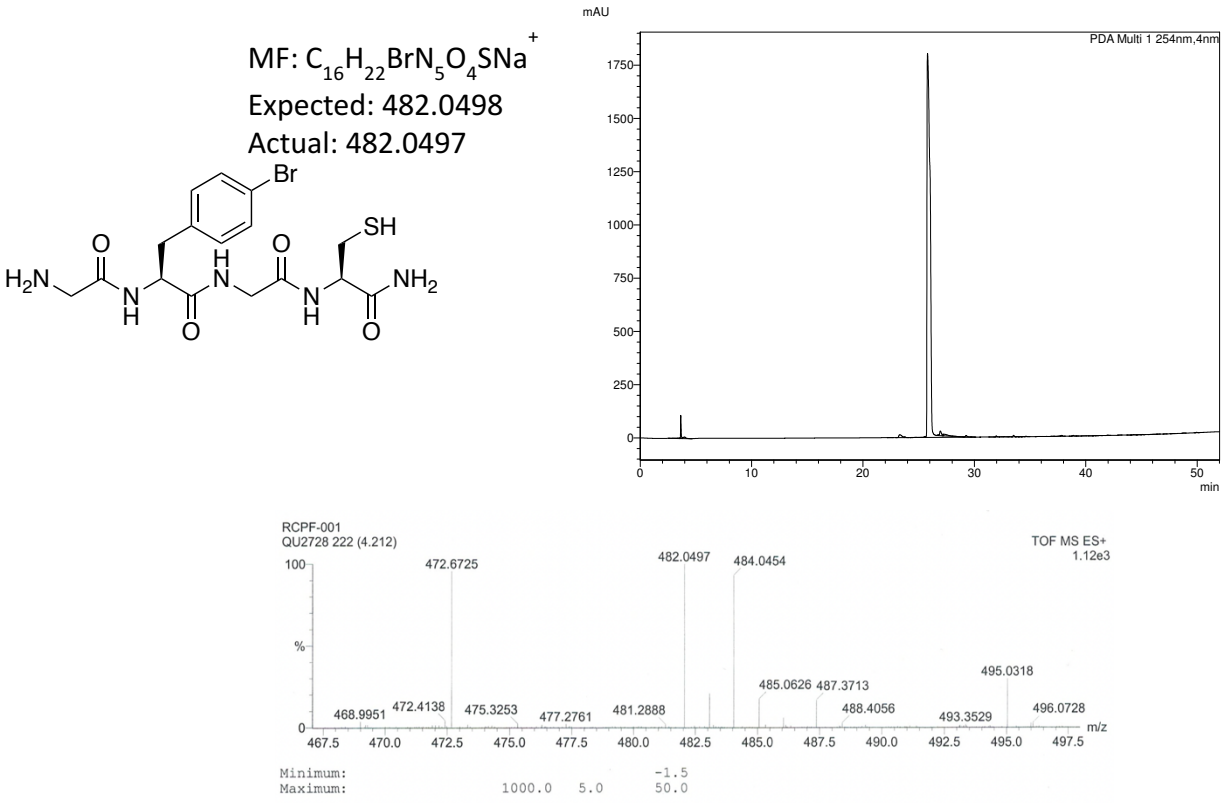

Figure 4.5: Structure and Characterization of GFGC (RCP) peptide fragment.

A: The terminal residue is a cysteine nucleophile and our isotopically labelled phenylalanine residue can be seen with a bromine at the *para* position. The atomic abundance of bromine is used here as a method to identify our peptide when performing MS experiments. The c-terminal of this peptide has been modified to an amide.

B: ***Analytical HPLC trace of RCP peptide fragment***.

Conducted using method A at a flow rate of 1mL/min at concentraion of 1mg/mL. The major product is denoted with a *. The product was characterized using ESI MS, and and peak before 10 minutes denotes a solvent peak. The product was calculated as >95% pure. Purification on this peptide was performed using method B semi prep HPLC. All purity tests were done at 254 nm and all impurities were accounted for.

C: MS characterization of cysteine peptide fragment

ESI MS analysis was performed on the purified product, and the identity of this peptide sequence was verified with a MNa^+ mass of 482.0497.

4.3 NAPQI Assay with Peptides

Each peptide sequence described in section 4.1 was incubated with 100μL freshly synthesized NAPQI solution at a concentration of 3.3 mM. A colour change was observed 60s after the addition of the NAPQI solution to our dissolved cysteine peptide in 1X pH=7.2 PBS buffer. This change in colour could be due to covalent binding of the thiol with NAPQI, causing rearomatization of the ring, making the colour clear. This type of colour change did not occur for any other peptide solution even after incubation and agitation for 24 hours. Binding of peptide to NAPQI was verified using HPLC and MS analysis. Positive binding results were seen only for the RCP peptide. HPLC analysis was done at 254 nm using method A and MS was performed as described in section 3.0. The change in colour and MS analysis indicated the presence of the NAPQI adduct validating our approach of the thiol nucleophile in the RCP sequence binding NAPQI *in vitro*. This further displays the selectivity of NAPQI with thiol nucleophiles compared to secondary amines (histidine), and validated our approach for characterization of peptide bound metabolite *in vitro*.

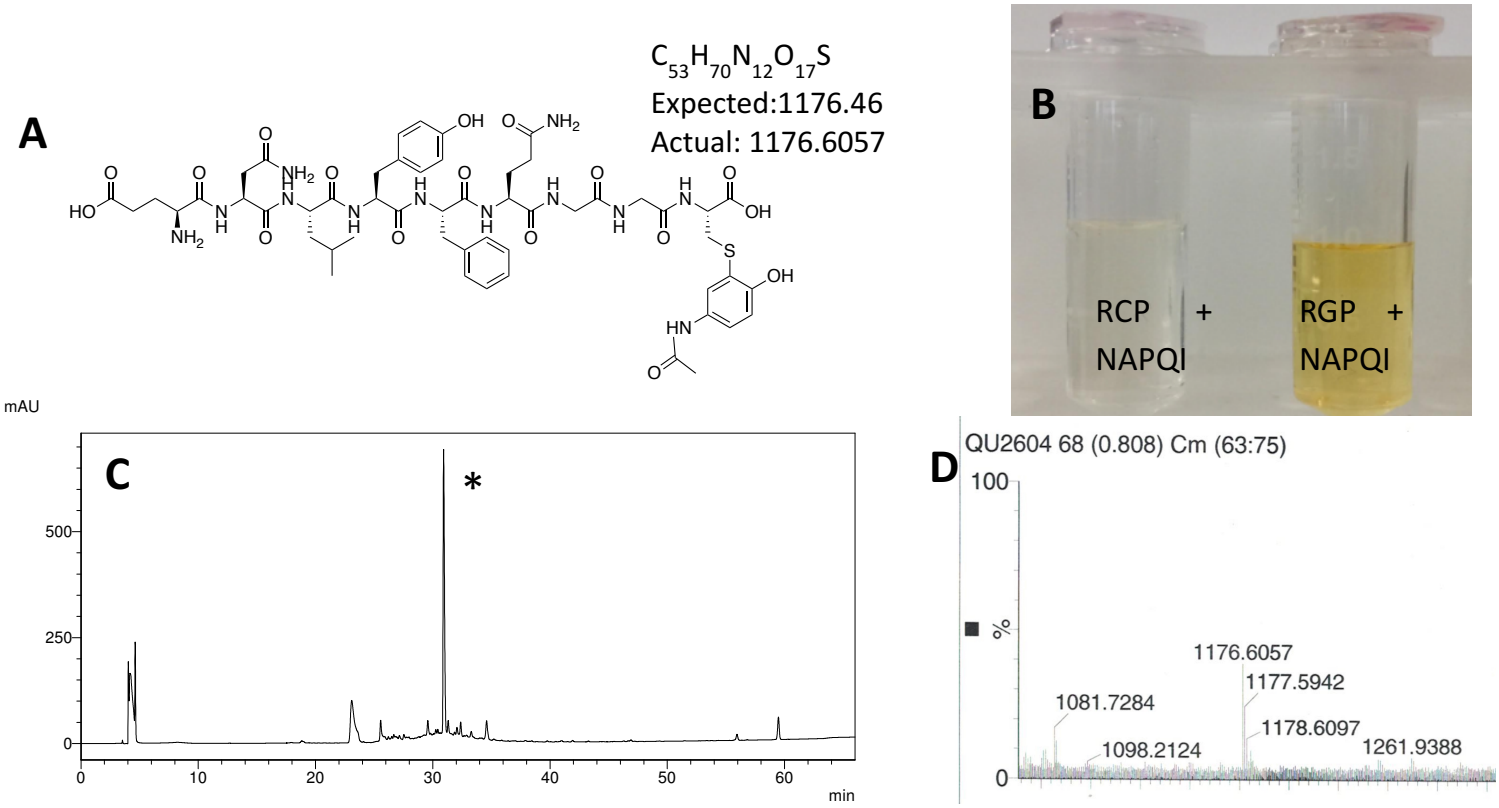

Figure 4.6: Structure and Characterization of peptide NAPQI conjugate:

A: The structure shown he is the proposed structure of the peptide sequence bound to NAPQI after incubation with the NAPQI solution. **B:** An image was taken of the reaction mixture upon addition of 3.3mM NAPQI solution (orange) in acetonitrile. In this picture, the RCP + NAPQI solution turns clear 60s after the addition of the NAPQI solution, whereas the RGP reaction remains orange. This color change may be an indicator of the NAPQI binding with the RCP peptide and returning to the colorless state of its starting material. **C:** HPLC trace of reaction between NAPQI and RCP peptide. * denotes peak that was collected and subjected to ESI MS analysis. **D:** ESI MS spectra of reaction between RCP and NAPQI, fragment detected with molecular mass of 1176.6057.

4.4 Coupling of Peptides to IONPs and NAPQI Assay Development

Commercially purchased IONPs were modified using EDC and NHS coupling chemistry as previously described. Since coupling times were relatively long (24h) NHS was used to prevent the formation of N-acylurea by-products (López-Alonso et al., 2009). Activated IONPs were treated with both peptide and targeting group overnight and were then washed until no UV absorbance caused by unreacted products was noted in eluent. Synthesized IONPs were then stored at 4°C in PBS buffer and this stock was used for all subsequent experiments. IONPs were incubated overnight with NAPQI and terminal peptide fragments were generated following TEV protease treatment (4.6A). In order to validate that cleavage of the TEV substrate (ENLYFQG|X) was possible off of the IONP, IONPs were incubated with TEV overnight in dialysis buffer (150mM NaCl, 50mM TRIS), in order to optimize TEV activity. This solution was then separated using a size exclusion column and was then subjected to HPLC analysis. HPLC analysis confirmed that a certain cleavage product was produced due to the presence of two major peaks at 16.5 and 20.2 minutes (figure 4.6B), where the latter peak's retention time is similar to our synthesized peptide fragment. Recovered peptide fragments displayed a strong absorbance at 254nm and 260nm and had similar retention times to our synthesized peptides fragments, indicating that some product was isolated from the IONP, although their identity was not confirmed. These results indicate that with optimization of conditions it may be possible to isolate peptide fragments from the surface of IONPs using TEV protease.

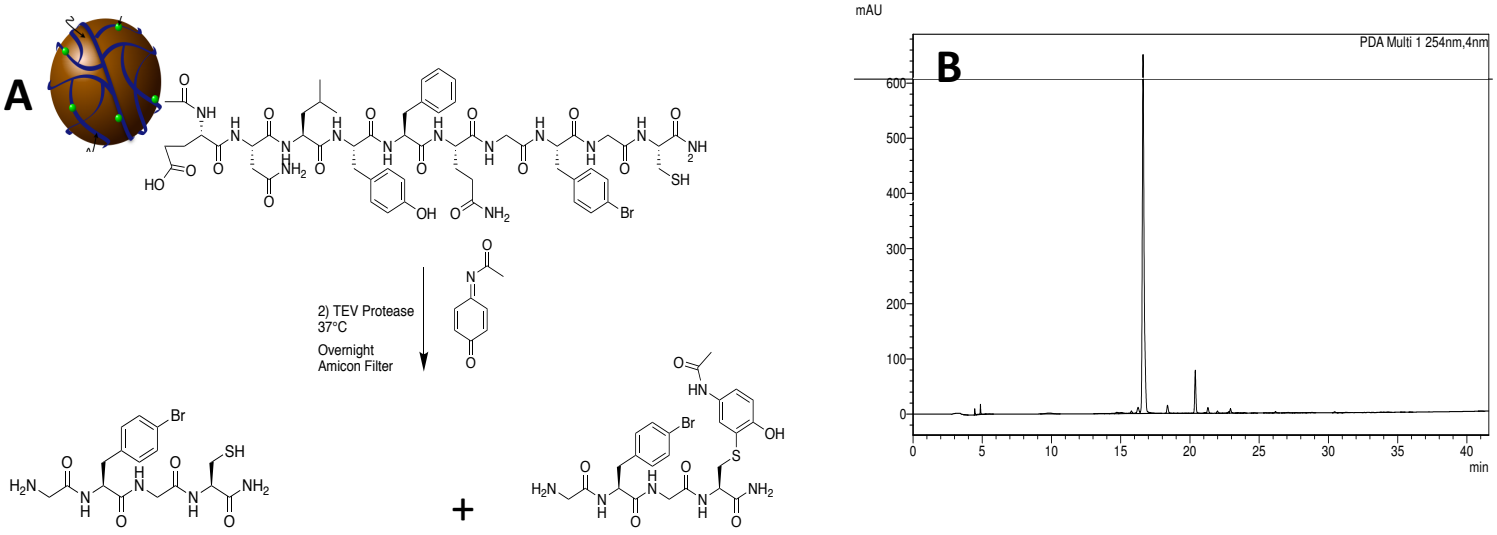

Figure 4.7: Assay for Isolation of Peptide-NAPQI:

A: Cysteine modified IONPs were incubated with 3.3mM NAPQI solution and treated with TEV protease. The proposed major products are the unreacted cysteine fragment and the peptide fragment bound to NAPQI. **B:** HPLC trace at 254nm of reaction mixture. The two major peaks (*) at 16.5 and 20.2 minutes correlate with our peptide sequence through a strong absorbance at both 254nm and 260nm.

4.5 IONPs Show a Change in T_2 MRI Signal in the Liver

MRI was used as a method to determine the optimal time of liver excision from the mouse in order to isolate the IONPs from the liver. T_2 Signal enhancement was used to indicate the presence of our IONPs. Stock commercially purchased IONPs show a rapid change in T_2 contrast signal in live mice (figure 4.7). Peptide modified untargeted IONPs show a similar rapid change in T_2 contrast signal as the unmodified commercially purchased IONPs (figure 4.8). Targeted peptide modified IONPs show a slower change in T_2 MRI signal compared to untargeted and purchased IONPs at 10 minutes post injection (figure 4.9). Although the different IONP types show different T_2 signals at 10 minutes it can be observed that our targeted IONP displays a significant contrast enhancement in the liver (figure 4.9). Percentage change in T_2 signal was calculated using the change in ROI intensity compared to the baseline (scan 1) in each image set, and the change in percentage is shown over a period of 90 min for each IONP type (figure 4.10). Data analysis indicates that after t=30 min there is no significant change in T_2 signal for all IONP types, and this time point was used for liver excision. All data plots are shown as an average of the liver ROI for two mice.

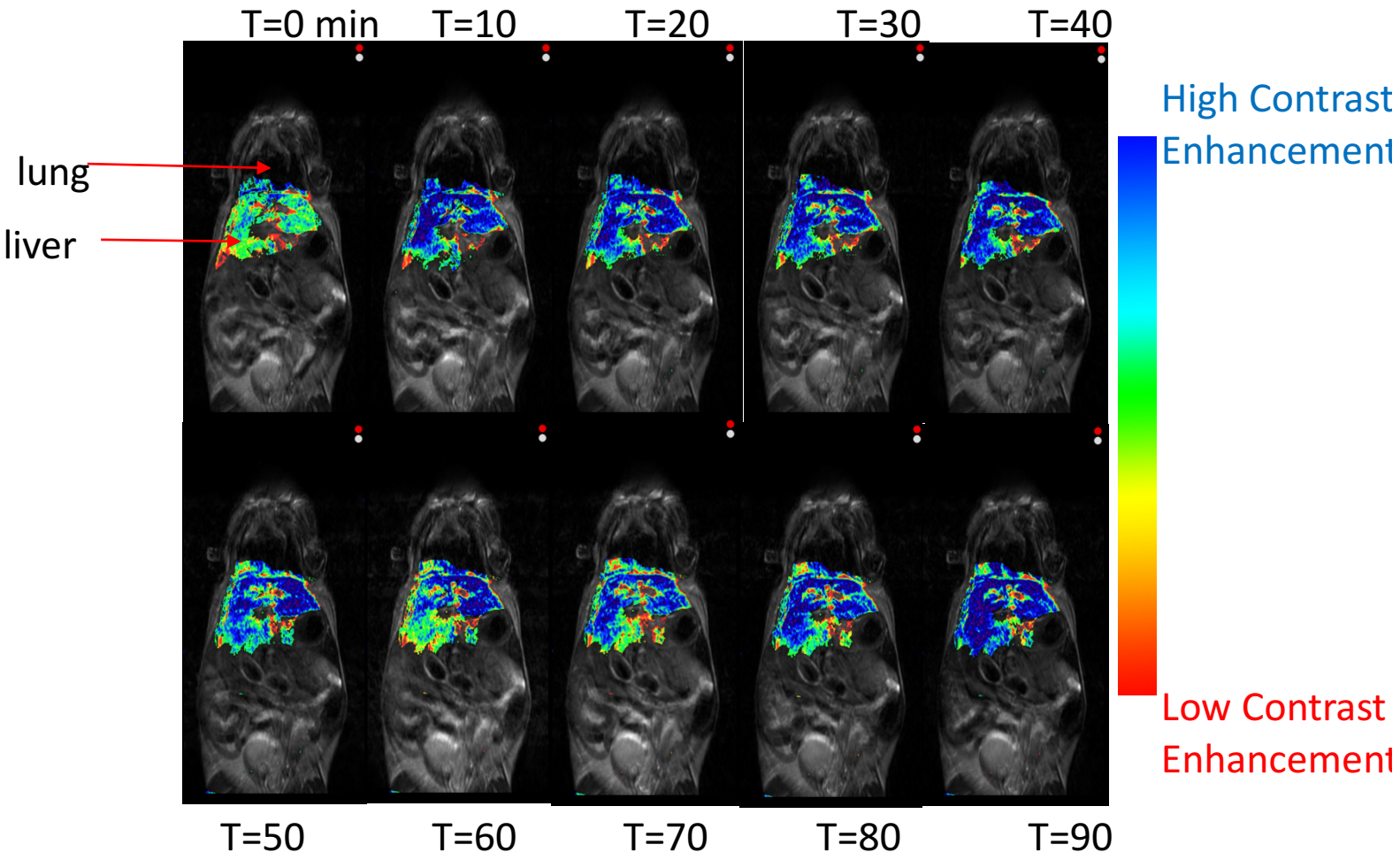

Figure 4.8: Stock IONPs show a rapid change in T_2 MRI signal in BALB/C mice.

Stock IONPs (0.75mg/100uL) were injected into live mice via tail vein and monitored using T_2-weighted MRI. The liver ROI is shown in colour and displays a change in T_2 signal. The first scan in this image set represents the baseline scan. At t=30 minutes post injection there is a plateau in the signal, and subsequent scans do not show a significant change in T_2 signal intensity. Red shows areas of lowest T2 intensity and blue areas show areas of strongest T2 intensity

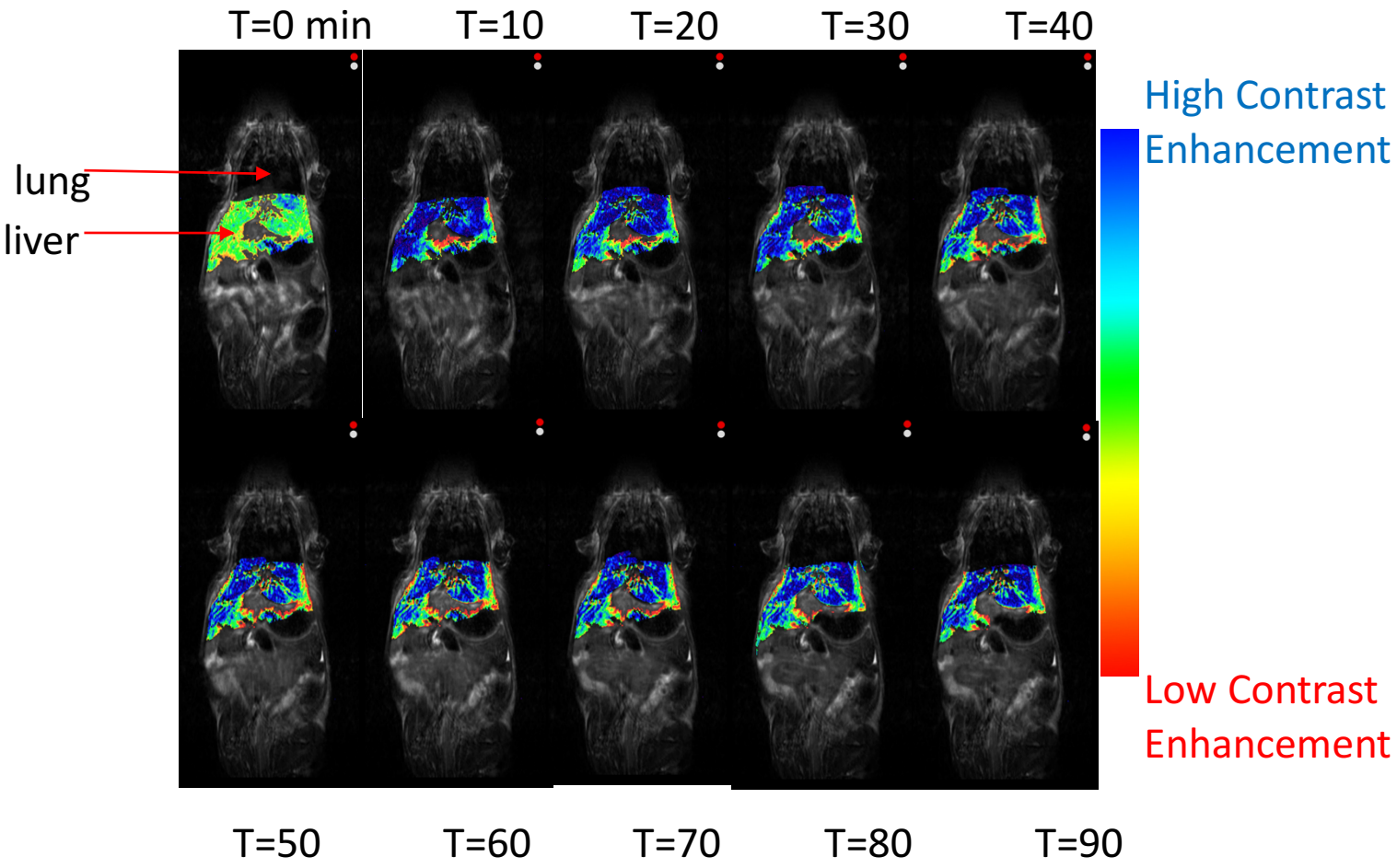

Figure 4.9: Peptide modified IONPs show rapid change in T_2 MRI signal.

Peptide modified IONPs (0.75mg/100uL) were injected into live mice via tail vein and monitored using T_2-weighted MRI. The liver ROI is shown in colour and displays a change in T_2 signal. The first scan in this image set represents the baseline scan. Scans show that the peptide modified IONPs have a rapid rate of reaching signal maximum. At t=30 minutes post injection there is a plateau in the signal, and subsequent scans do not show a significant change in T_2 signal intensity. Red shows areas of lowest T2 intensity and blue areas show areas of strongest T2 intensity

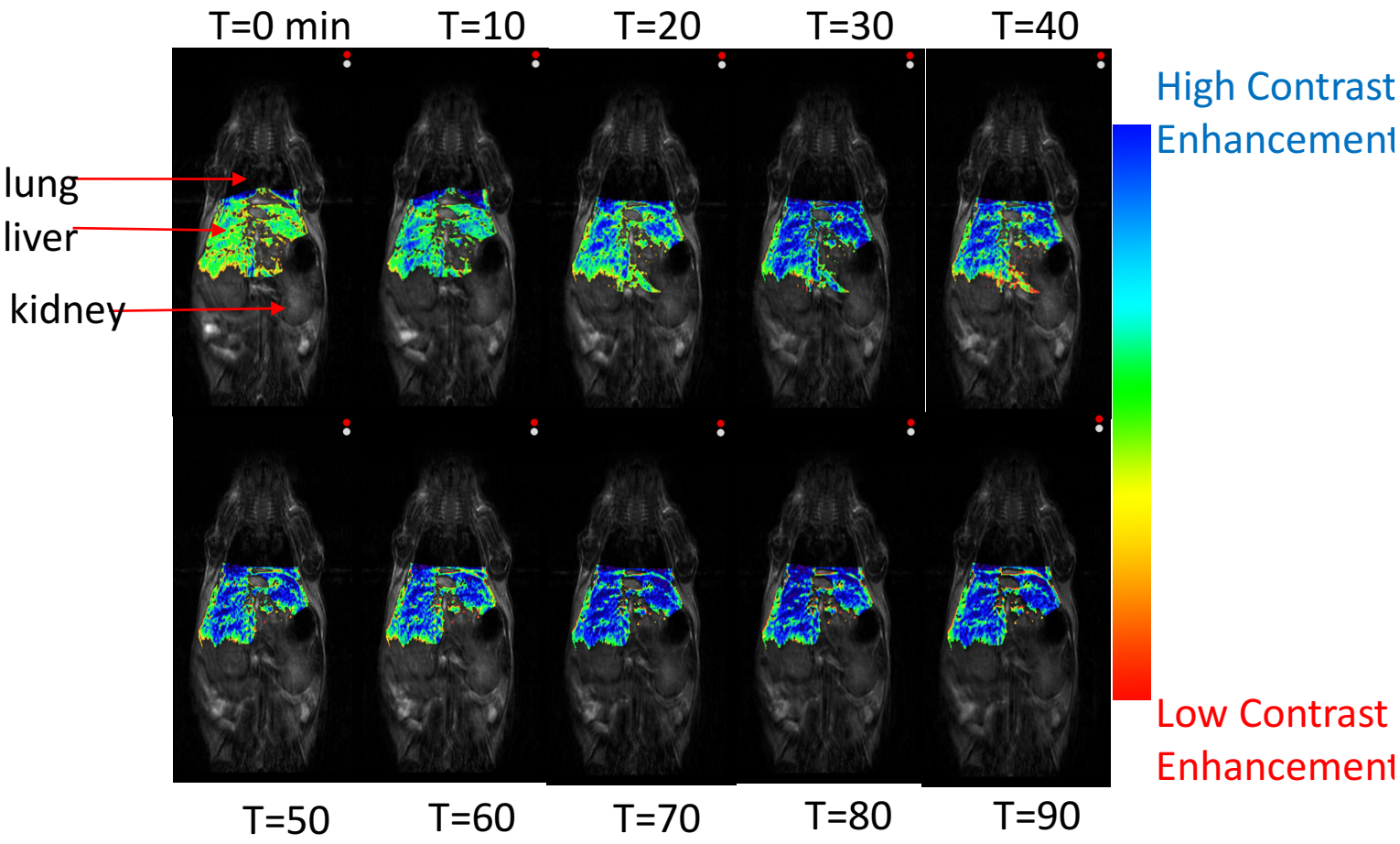

Figure 4.10: Targeted IONPs show a slow change in T_2 MRI signal in BALB/C mice.

Targeted IONPs (0.75mg/100uL) were injected into live mice via tail vein and monitored using T_2-weighted MRI. The liver ROI is shown in colour and displays a change in T_2 signal. Scans show that the targeted IONPs have a slow rate of reaching signal maximum compared to stock and peptide modified IONPs. The first scan in this image set represents the baseline scan. At t=30 minutes post injection there is a plateau in the signal, and subsequent scans do not show a significant change in T_2 signal intensity.
Red shows areas of lowest T2 intensity and blue areas show areas of strongest T2 intensity

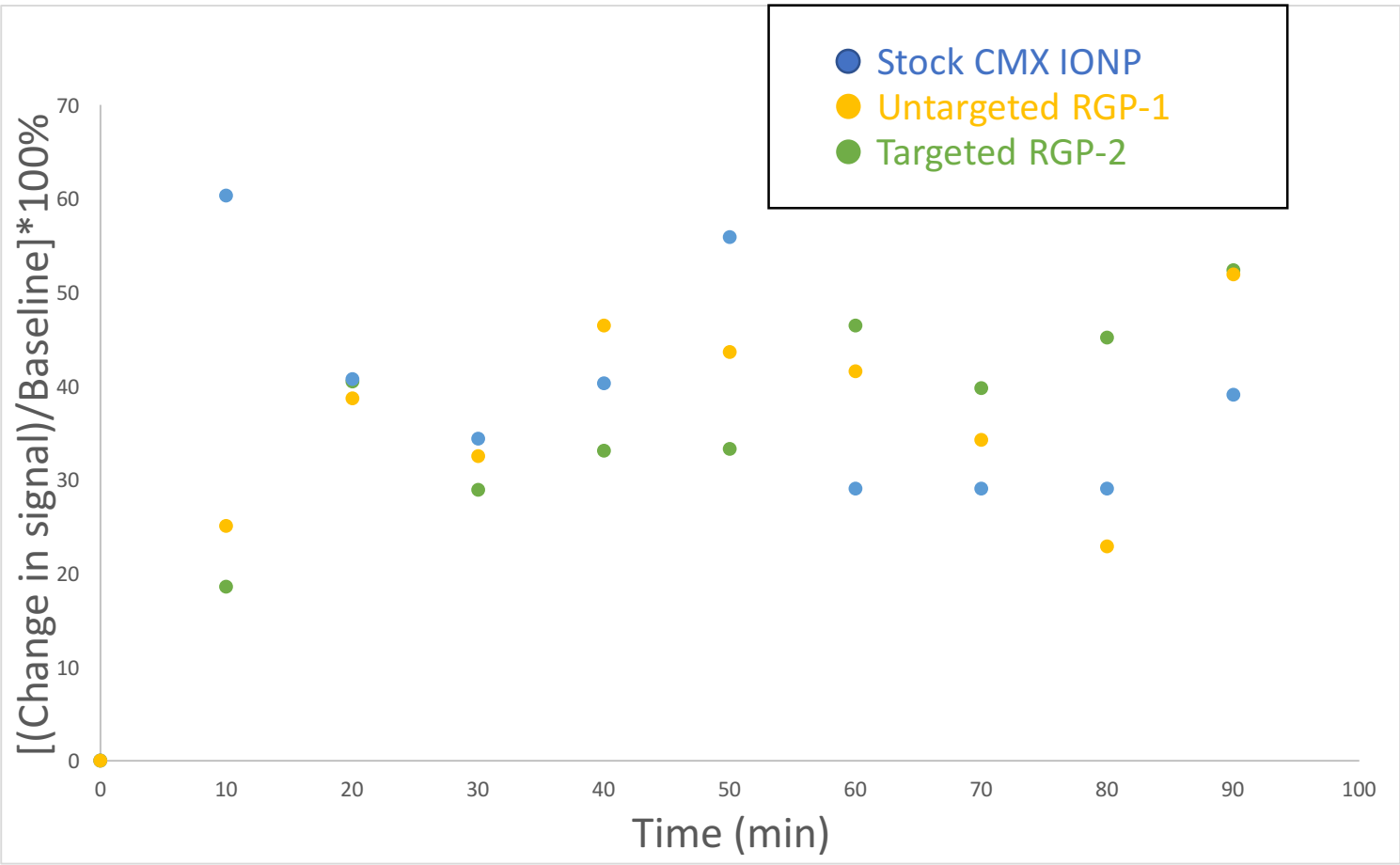

Figure 4.11: Stock and Targeted IONPs display a different rate in T_2 signal change in MRI 30 minutes post injection.

Data was generated using Vivoquant ® ROI image analysis. Data shows that the targeted IONPs have a slow rate of reaching signal maximum compared to stock and untargeted IONPs. At t=30 minutes post injection there is a plateau in the signal, and subsequent scans do not show a significant change in T_2 signal intensity. Data shows percentage change in T signal where the baseline scan is the 0 signal. The signal strength after 30 minutes between targeted, stock, and untargeted is very similar, meaning the concentration of IONPs in the liver after this time point are similar. Each time point is the average of the ROI between two mice of the specific IONP type.

4.6 Extraction of NP from Liver and Treatment with TEV Protease

Mice were treated with 100μL of 0.75 mg/100μL IONPs via a tail vein injection in saline. Mice were euthanized 30 minutes after injection of probe as this time displayed optimal T_2 signal as determined by our MRI studies (4.5). Isolated livers were homogenized using RIPA buffer and were eluted through a magnetic field capturing our IONPs from the homogenate. Initial homogenization and isolation protocols lead to no IONPs being recovered, observed through no UV absorbance from eluent of the magnetic column. In order to increase the concentration of IONPs present in the liver of mice at 30 minutes the concentration of injected IONPs was increased to 7.5mg/100μL maintaining the injection volume of 100μL. It was hypothesized that increasing the concentration of injected IONPs would lead to more IONPs being recovered from the liver giving a detectable response.

Following treatment of mice with the increased dose of IONPS, livers were extracted and homogenized as described before. IONPs were extracted from the liver using magnetic separation and treated with TEV protease. Expected peptide fragments from eluent were recovered using an Amicon size exclusion column and diluted to 1mL and subjected to HPLC analysis. The HPLC spectra (figure 4.11B) shows the trace obtained from the recovered peptide after treatment with TEV. The large peak denoted with a * had a peak profile with strong absorbance at 254nm and 260nm and a similar elution time to our chemically synthesized full peptide fragments (figure 4.11A).

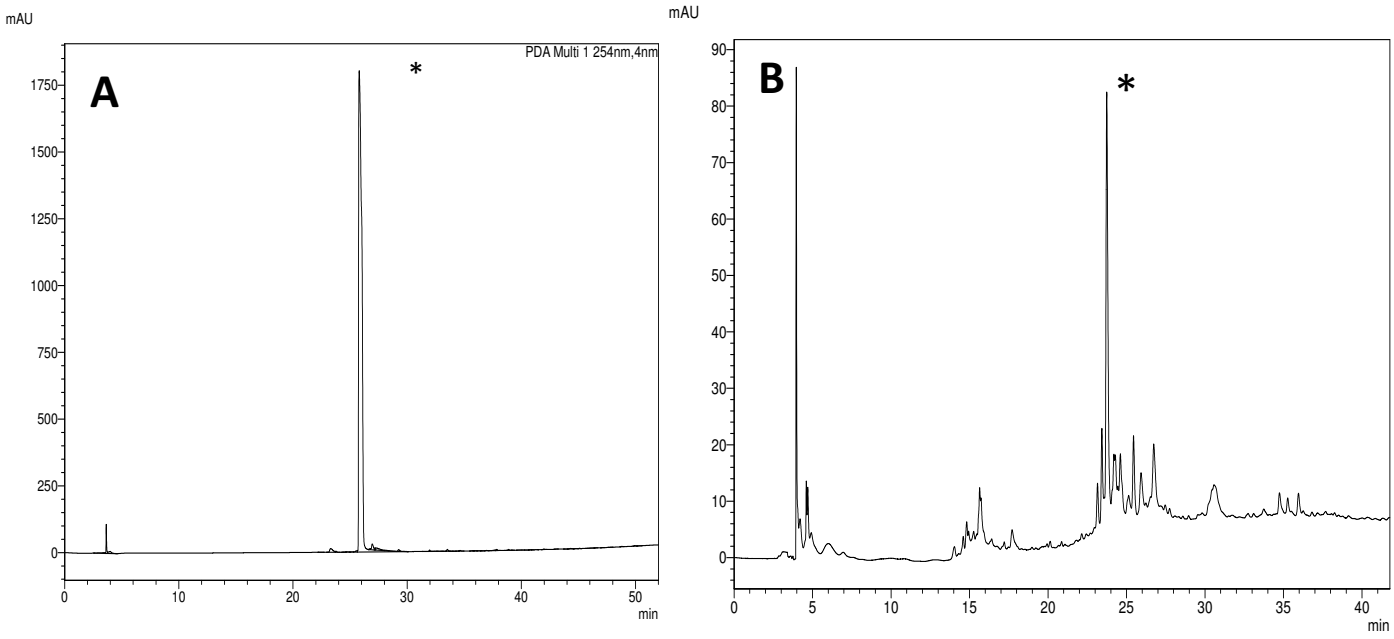

Figure 4.12: HPLC trace of NPs isolated from liver and treated with TEV protease.

A: HPLC trace at 254nm of peptide standard with major peak displayed at 25.8min.
B: Recovered IONPs from mouse liver were treated with TEV protease and subjected to HPLC analysis. TEV treated IONPs gave a detectable HPLC signal and there is a presence of a peak (*) that has a similar elution time to our synthesized standards. The peak at 23 minutes also displayed strong absorbance at both 254nm and 260nm similar to our synthesized peptides (A).

CHAPTER 5.0 DISCUSSION OF RESULTS

5.1 CHARACTERIZATION OF NAPQI-THIOL BINDING

GSH is the known endogenous detoxifying agent for APAP overdose, and covalently binds to NAPQI *in vivo*. Once GSH stores have been depleted then NAPQI binds endogenous proteins leading to hepatotoxic events (figure 5.1). GSH binding to NAPQI was confirmed using LC/MS characterization showing the presence of the NAPQI-GSH adduct M^+:456.1315. This data showed that our synthesis of NAPQI was successful and that we could trap this metabolite using a thiol nucleophile. LC/MS data was optimized for detecting covalent modification of this metabolite for future *in vivo* investigations. Once this binding and synthesis was confirmed further investigations were carried out to determine the reactivity of NAPQI to other nucleophiles.

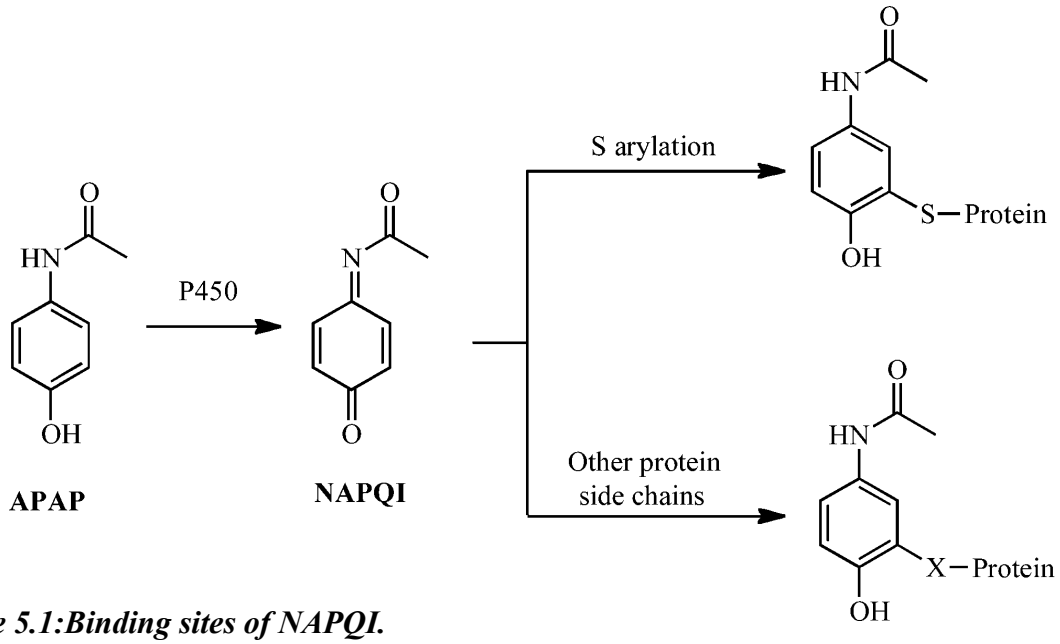

Figure 5.1:Binding sites of NAPQI.
Following Phase I metabolism of APAP the reactive metabolite NAPQI can covalently modify proteins. The sites of protein modification have been shown to be the *ortho* hydroxyl site. S arylation refers to the typical binding site of thiol nucleophiles with NAPQI. The other protein side chains refer to the unknown or undiscovered proteins which may bind to NAPQI leading to hepatotoxic events. Our work will take both binding pathways to determine the reactivity of NAPQI *in vivo*. Adapted from Leeming, Gamon, Wille, Donald, & O'Hair, 2015a.

5.2 Cysteine Peptides Bind NAPQI *in vitro*.

Peptides bearing C-terminal nucleophiles and C-terminal amides were synthesized to explore their ability to trap the reactive metabolite NAPQI. It was shown that NAPQI reactivity was selective for thiols and not secondary amines (figure 4.5). This reactivity with thiols can be attributed to NAPQI being a good Michael acceptor and a soft electrophile. Reactivity with C-terminal histidine or glycine were not observed. Our control glycine peptide sequence did not react with NAPQI, as shown through MS analysis, indicating that no other residue on our peptide sequence reacted with the metabolite. A colour change was observed almost immediately upon addition of NAPQI to our cysteine peptide solution. This colour change can be attributed to the fact that upon binding of the thiol to the NAPQI metabolite, we observe rearomatization of the product, which may be the cause of the colour change. The selectivity for thiol nucleophiles also occurs endogenously where NAPQI is detoxified by GSH and its hepatotoxicity stems from covalently modifying cysteine active site proteins *in vivo* (Stamper, Mohar, Kavanagh, & Nelson, 2011).

5.3 Design of a Hepatocyte Targeting Group

Tageting of IONPs to heptaocytes was done by employing a galactose-PEG moiety (PEG-GAL) (synthesis described in section 3.0). The hypothesized role of the PEG-GAL moiety is to allow uptake into hepatocytes. Our hepatocyte targeting group allowed entry of our IONP into the liver of live mice as shown in figure 4.20. The synthesis and design of the PEG-GAL moiety was taken from (Zeng, Sun, Zhang, & Zhuo, 2009), and has been used previously to show strong uptake in the hepatocytes. In the paper by (Bartczak, Baradez, Goenaga-Infante, & Marshall, 2015) they show how surface modifications of NPs can change their properties and even reduce overall toxicity of the NPs. This result was shown in our IONP *in vivo* results as our probe showed strong

contrast enhancement in the liver and the presence of the targeting grouped slowed the rate of uptake of the IONP *in vivo*.

The hepatocyte targeting group was rationally designed with two major components; a large PEG linker and a galactose moiety. The use of a single galactose on our targeting group serves to guide our IONP to hepatocytes, and the PEG linker acts to reduce the speed at which these IONPs circulate in the vasculature (M. H. Lee et al., 2012). The galactose with a glycosidic bond to the PEG linker has been used extensively for hepatocyte targeting due to the robustness of the galactose targeting and the relatively stable nature of the compound *in vivo* (Arami et al., 2015; M. H. Lee et al., 2012). The stability of our targeted IONPs can also be shown through the increased darkening in the liver after their injection.

5.4 The Use of TEV and RCP NP in the Development of a Pull-Down Assay for NPs

A TEV protease assay was designed in order to cleave the peptide sequence from the NP and facilitate MS analysis. TEV protease is a 3C type protease which is frequently used in various biochemical applications. The TEV protease is structurally similar to the serine proteases such as trypsin and chyomotripsin, but bearing a thiol cysteine in the active site (Ryan & Flint, 1997). Cys^{151} is located at the interface between the domains (Phan et al., 2002). TEV has been used regularly as a protease in biological assays and is found to be quite robust and selective for its substrate, ENLYFQ|X. Our peptide treated with TEV protease did produce a cleavage product observed by HPLC. The retention time of this peak on HPLC was similar to our control peptide standards and also displayed similar absorbance at 254nm and 260nm.

5.5 IONPs as *in vivo* Tracking Agents

Covalent modification of proteins found in the mitochondria of hepatocytes has been suggested to

be the major cause of hepatotoxic events induced by APAP (Stamper et al., 2011). This covalent modification leads to loss of function and a large amount of oxidative stress on the cell. T_2 MRI was used to determine the time of liver excision. The amount of IONP in liver was correlated to the T_2 signal exhibited by the IONPs as an increase in contrast enhancement, or a darkening. It was shown that our NP produced no initial contrast signal for a 100μL injection of 0.375mg/100μL of IONP per 20g mouse. The work done by (Arami et al., 2015) showed that with CMX-IONPs a change in T_2 signal is noticed with a 0.75 mg/100μL injection of IONP per 20 g mouse. After changing our injection concentration to 0.75 mg IONP per 100 μL of sterile saline, we noticed a significant change in T_2 signal through an increase in contrast enhancement, or darkening when compared to control baseline scans. This change in signal was observed in all three imaging types: stock (unmodified IONPs), targeted (peptide and targeting group modified), and untargeted (only peptide modified), although the different formulations displayed different rates of contrast enhancement. A high contrast enhancement can be seen for all image types in figures 4.7, 4.8, and 4.9.

Previous studies have shown that the optimal change in contrast is directly correlated with the surface modifications and the type of IONP (Wilhelm et al., 2016). It has been shown that different surface modifications of IONPs can cause different rates of contrast enhancement due to the rate of entry into the target tissue (Arami et al., 2015). At 10 minutes post injection, we observe a large increase in T_2 signal in stock and untargeted IONPs compared to targeted IONPs (figure 4.10). This sudden increase in signal is hypothesized to be due to a large influx of the probe in the vasculature but not necessarily in the hepatocytes, our target cells (Bartczak et al., 2015). ROI data was calculated by averaging the liver signal for two mice, and displayed that targeted IONPs show

a 30% lower T_2 signal in the liver than stock IONPs at 10 minutes. The percentage change of signal compared to baseline in the three IONP formulations was the same approximately 30 minutes post injection and did not show a substantial change in contrast enhancement in subsequent time points. Due to the plateau in signal 30 minutes after injection, this time point was used as the optimal time point for liver excision and for *ex vivo* studies.

5.6 Concentrated IO*NPs Isolated from Liver Homogenate*

Initial IONP injections at 0.75mg/mouse did not display recovery of IONPs after homogenization and magnetic separation of liver homogenate. Since the presence of our IONP was also detected via T_2 MRI it can be concluded that our IONPs do show localization in the liver. After substantial optimization of homogenization and injection parameters of IONPs, a concentration of 7.50mg/mouse per 100 uL injection and increased homogenization times to 3 rounds of 3 minutes, the presence of IONPs was detected. This means that there needs to be a total injection of 7.50 mg/mouse in order to get a sufficient extraction of NPs for minimum IONP recovery. In order for this method to be optimized and be useful for characterization studies the amount of IONP recovered needs to be increased. Further increasing of the dosage of IONPs may not be promising as higher doses may have toxic side effects (Arami et al., 2015), (Wilhelm et al., 2016). After treatment of these IONPs with TEV protease we were able to detect an HPLC signal with similar retention times as our synthesized peptide standards, indicating the presence of our isolated desired fragment (figure 4.11). Although we were not able to successfully characterize our isolated fragment, with optimized LC/MS protocols the recovered fragment may be characterized in order to validate this approach. Overall if we improve the number of IONPs recovered, we can increase the concentration of peptide fragment recovered. Through optimization of LC/MS parameters and

increased peptide fragment concentration we may be able to characterize peptide fragments recovered from liver homogenate.

5.7 Significance of Findings

In our initial hypothesis, we proposed to design an IONP that can be injected into live mice which would be functionalized using a peptide sequence and a hepatocyte targeting group. The rational peptide design consisted of various endogenous nucleophiles that would react with electrophilic drug metabolites. In this study, we were able to successfully synthesize three peptide sequences bearing different C-terminal residues. These peptides were then incubated with a synthesized NAPQI solution to determine reactivity to the metabolite. Selectivity for thiol nucleophiles was shown over secondary amines. These peptides were then successfully coupled to the surface of IONPs. An assay was developed in order to selectively cleave these peptides from the IONP using TEV protease. The TEV protease substrate (ENLYFQG|X) was incorporated in our peptide sequence, and through HPLC analysis we confirmed that some fragment was recovered upon treatment with TEV protease. This work shows the ability for the proteases to act on IONPs, and their ability to recognize and cleave their substrate even when they are conjugated to the surface of an IONP. The use of these IONPs *in vivo* was also investigated through monitoring them *via* T_2 MRI, showing their ability to localize in the liver.

Although this study falls short of characterizing the fragments recovered from the liver of live mice, further optimization is necessary in order to characterize the metabolites recovered in order to validate the method in this study. Overall, we developed a method to investigate binding of drug metabolite NAPQI to peptide sequences *in vitro*, and developed an assay to potentially

investigate the binding of this metabolite to peptides *in vivo*. Taken together our work shows that there still remains a lot of work necessary to develop a method for characterizing these metabolites *in vivo*, but there is a large need to develop a method to characterize reactive metabolites *in vivo* in order to investigate their innate toxicities and to implement these findings in the drug development process.

6.0 Limitations and Future Directions

6.1 Improving Methods for NP Recovery

A lot of work has been done in investigating NPs and their delivery efficiency (Wilhelm et al., 2016). As seen in our work it was necessary to increase the dose of NP to get enough recovery from the liver to get a detectable response. Wilhelm et al. discuss how NPs circulate and the number of NPs that reach a specific target site is much lower than the amount that is injected. As seen in our MRI experiments NPs circulate rapidly (Figure 4.22), and remain in the animal for large periods of time, in this case over 1h. A major limitation of our work is the small number of NPs recovered after excision of the liver and also the increase in dosage to get a detectable response. There may be toxic effects of increasing NP dosage that are not detected, making this dosage increase a non-viable way of increasing NP recovery.

Optimization of the homogenization protocol such as increased sonication times, and potentially pooling livers of the same study together may increase the number of IONPs retained. Another method to improve the retention of IONPs in the liver may be to increase the hydrodynamic size of the IONP, since ours are 50nm these may be too small to recover. Increase the size of the IONPs would increase their retention in the liver (Arami et al., 2015). The liver retention may also be improved by the optimization of targeting groups to improve selectivity of hepatocytes. Since most receptors on hepatocyte surfaces have high selectivity for galactose modified proteins, it may

be feasible to increase the number of targeting groups on the surface of the IONPs, ultimately improving receptor mediated entry into cells. A major caveat of galactose mediated entry into hepatocytes is that liver macrophages also bind to galactose modified proteins and molecules, as such this method does not necessarily improve selectivity of hepatocytes over macrophages. As such increasing the number of galactoses on the surface of our IONP may improve liver selectivity but not necessarily hepatocyte selectivity (Acta, Bba, & Microscop, 1985). Overall by increasing the size of IONPs and by improving the design of our targeting group to incorporate more than one galactose moiety per PEG linker, we may be able to improve liver retention and ultimately recovery of these IONPs after excision and homogenation of the liver. If increased retention in the liver is seen but only with increased macrophage activity, treatment with n-acetylgalactosamine may reduce binding of IONP to macrophages while only slightly reducing binding to hepatocytes (Acta et al., 1985).

This work has shown that NPs conjugated to a PEG targeting group show slower uptake and slower rates of signal increase in the liver. This discovery compliments the discussion by Wilhelm et al., where they show that NPs circulate rapidly in the vasculature, making it difficult for them to enter the targeted cells. Willhelm et *al*. suggest that introduction of PEG on the surface of these NPs reduces the speed of circulation, increasing the number of NPs entering the targeted cell. The suggest that by introducing a large number of small PEG chains, the NP speed of dispersion in the vasculature is reduced leading to a larger number of NPs entering the targeted cell. Although we implemented a PEG chain on our surface, a way to further increase cell entry would be to incubate our NPs after surface modification with smaller PEG chains that would react with carboxy groups on the surface of our NPs that are unconjugated. These PEG groups could be designed such that they are smaller in size than the peptides, so they do not interfere with peptide-metabolite binding

but still influence the circulation of these IONPs *in vivo*. These smaller PEG groups would reduce the speed of the NPs in the vasculature and allow adequate entry of the NPs into the hepatocyte, giving us more NPs recovered after excision and homogenization of the liver.

6.1 LC/MS Characterization and Lower Limit of Detection

A major limitation of this work is the lack of characterization of the surface of the IONPs. Once peptide and targeting group are coupled to the IONP, the level of substitution is difficult to quantify. In the synthesis of our RCP IONP it may be possible to approximate the amount of peptide present on the surface with Ellman's reagent (Moser et al., 2015). By using an Ellman's reagent we could determine the lower limit of detection for an LC/MS protocol, and quantify the amount of IONP necessary for a detectable response. This could be done by having different concentrations of RCP modified IONPs ranging from large to small, and using the lower concentrations to determine how much give a detectable response. The lower end could then be treated with TEV protease and subjected to LC/MS analysis to see if an adequate LC and MS signal is obtained. This data would determine how much IONP needs to be injected into the mouse in order to isolate an amount that can be run through an LC/MS protocol. Since a major limitation shown in our results was that the isolated IONPs were very dilute and produced a very low signal to noise ratio, determining how much of the IONP is necessary to give an adequate LC/MS signal would optimize the injection concentration and the recovery from the liver. Although this method does not overcome the obstacle of increasing the recovery, it does quantify how much of the IONP needs to be recovered in order to achieve a detectable response.

6.3 Future Directions

There are many known hepatotoxins that have not just one but a variety of reactive metabolites, which are still only hypothesized but have not yet been characterized. Figure 6.1 shows a few examples of drugs that could potentially be characterized using the method described in this study.

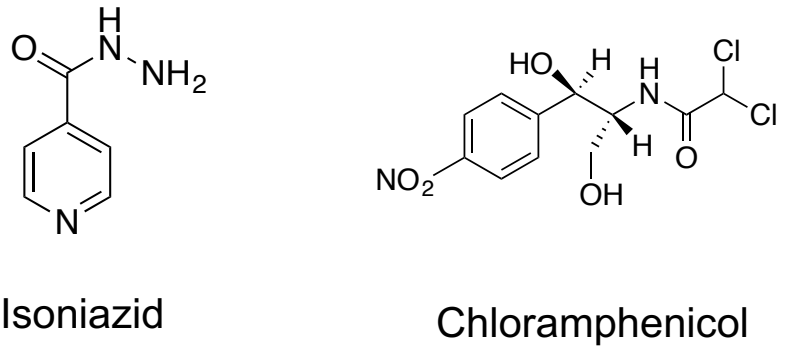

Figure 6.1: Future drug targets to study with the electrophilic IONP system.
Isoniazid (left) is a known tuberculosis treatment and chloramphenicol (right) is a commonly used antibiotic both in clinical and non-clinical research. These drugs have many hypothesized metabolic pathways, including potential protein targets. The electrophilicity of these drugs varies from NAPQI and has susceptibility to react with non-cysteine endogenous nucleophiles.

Isoniazid shown in figure 6.1 has many known metabolic pathways and many reactive intermediates as it is metabolized and removed from the body. As a commonly used TB treatment it has a high incidence of hepatotoxic events. Its reactive metabolite is known to react with lysine active site proteins. In order to characterize its reactive metabolites, we could implement a lysine bearing IONP and use the same TEV pull down assay to characterize the metabolite. Chloramphenicol is another known hepatotoxin and is another historically used drug whose hepatotoxicity is still not well understood. To investigate the reactivity of chloramphenicol *in vivo*, we could implement a NP which has all three nucleophile bearing peptides coupled to it, and then used our TEV assay to pull out all of the sequences. We could then perform LC/MS experiments

to determine which nucleophile binds to the reactive metabolite using CID, and look for the presence of an M+2 peak.

7.0 REFERENCES

Acta, B., Bba, E., & Microscop, E. (1985). Binding activity of macrophages is lost by EDTA treatment, *847*, 108–114.

Alempijevic, T., Zec, S., & Milosavljevic, T. (2017). Drug-induced liver injury: Do we know everything? *World Journal of Hepatology*, *9*(10), 491. https://doi.org/10.4254/wjh.v9.i10.491

Arami, H., Khandhar, A., Liggitt, D., & Krishnan, K. M. (2015). In vivo delivery, pharmacokinetics, biodistribution and toxicity of iron oxide nanoparticles. *Chem. Soc. Rev.*, *42*(12), 4906. https://doi.org/10.1039/C5CS00541H

Bartczak, D., Baradez, M.-O., Goenaga-Infante, H., & Marshall, D. (2015). Label-free monitoring of the nanoparticle surface modification effects on cellular uptake, trafficking and toxicity. *Toxicol. Res.*, *4*(1), 169–176. https://doi.org/10.1039/C4TX00105B

Bessems, J. G., Te Koppele, J. M., Van Dijk, P. A., Van Stee, L. L., Commandeur, J. N., & Vermeulen, N. P. (1996). Rat liver microsomal cytochrome P450-dependent oxidation of 3,5-disubstituted analogues of paracetamol. *Xenobiotica*, *26*(0049–8254), 647–666. https://doi.org/10.3109/00498259609046740

Blair, I. A., Boobis, A. R., Davies, D. S., & Cresp, T. M. (1980). Paracetamol oxidation: synthesis and reactivity of N-acetyl-p-benzoquinoneimine. *Tetrahedron Letters*, *21*(51), 4947–4950. https://doi.org/10.1016/S0040-4039(00)71162-2

Bouvy, J. C., Bruin, M. L. De, & Koopmanschap, M. A. (2015). Epidemiology of Adverse Drug Reactions in Europe : A Review of Recent Observational Studies. *Drug Safety*, 437–453. https://doi.org/10.1007/s40264-015-0281-0

Brodie, B. (n.d.). 1, 1949, 58–67.

Bromer, M. Q., & Black, M. (2003). Acetaminophen hepatotoxicity. *Clinics in Liver Disease*, *7*(2), 351–367. Retrieved from http://www.ncbi.nlm.nih.gov/pubmed/12879988

Busman, M., Knapp, D. R., Schey, K. L., & Smith, R. (1994). Observation of large multimers in the electrospray ionization mass spectrometry of peptides. *Rapid Communications in Mass Spectrometry*, *8*(2), 211–216. https://doi.org/10.1002/rcm.1290080217

Caulín, C., Salvesen, G. S., & Oshima, R. G. (1997). Caspase Cleavage of Keratin 18 and Reorganization of Intermediate Filaments during Epithelial Cell Apoptosis, *138*(6), 1379–1394.

Centers, C., States, U., Ostapowicz, G., Fontana, R. J., Schiødt, F. V, Larson, A., … Han, S. H. B. (2002). Article Results of a Prospective Study of Acute Liver Failure at 17 Tertiary, (15), 947–955.

Chandrasekharan, N. V, Dai, H., Roos, K. L. T., Evanson, N. K., Tomsik, J., Elton, T. S., & Simmons, D. L. (2002). COX-3, a cyclooxygenase-1 variant inhibited by acetaminophen and other analgesic/antipyretic drugs: cloning, structure, and expression. *Proceedings of the National Academy of Sciences of the United States of America*, *99*(21), 13926–31. https://doi.org/10.1073/pnas.162468699

Chen, B. (2010). Surface Plasmon Resonance. *Methods in Molecular Biology*, *627*(1), 147–155. https://doi.org/10.1007/978-1-60761-670-2

Chen, M., Tung, C. W., Shi, Q., Guo, L., Shi, L., Fang, H., … Tong, W. (2014). A testing strategy to predict risk for drug-induced liver injury in humans using high-content screen assays and the "rule-of-two" model. *Archives of Toxicology*, *88*(7), 1439–1449. https://doi.org/10.1007/s00204-014-1276-9

Chughlay, M. F., Kramer, N., Werfalli, M., Spearman, W., Engel, M. E., & Cohen, K. (2015). N -acetylcysteine for non-paracetamol drug-induced liver injury : a systematic review protocol. *Systematic Reviews*, 1–6. https://doi.org/10.1186/s13643-015-0075-6

Church, R. J., Watkins, P. B., & Law, H. Y. S. (2017). The transformation in biomarker detection and management of induced liver injury, (February), 1–9. https://doi.org/10.1111/liv.13441

Clarke, P., & Tyler, K. L. (2009). Apoptosis in animal models of virus-induced disease. *Nature Reviews Microbiology*, *7*(2), 144–155. https://doi.org/10.1038/nrmicro2071

Conde, J., Dias, J. T., Grazú, V., Moros, M., Baptista, P. V, & de la Fuente, J. M. (2014). Revisiting 30 years of biofunctionalization and surface chemistry of inorganic nanoparticles for nanomedicine. *Frontiers in Chemistry*, *2*(July), 48. https://doi.org/10.3389/fchem.2014.00048

Dahlin, D. C., & Nelson, S. D. (1982). Synthesis, decomposition kinetics, and preliminary toxicological studies of pure N-acetyl-p-benzoquinone imine, a proposed toxic metabolite

of acetaminophen. *Journal of Medicinal Chemistry*, *25*(8), 885–886. https://doi.org/10.1021/jm00350a001

Dalvie, D., Kalgutkar, A. S., & Chen, W. (2017). Practical approaches to resolving reactive metabolite liabilities in early discovery Practical approaches to resolving reactive metabolite liabilities in early discovery, *2532*(June). https://doi.org/10.3109/03602532.2014.984813

David Josephy, P. (2005). The molecular toxicology of acetaminophen. *Drug Metabolism Reviews*, *37*(4), 581–594. https://doi.org/10.1080/03602530500205200

Davies, N. M., Good, R. L., Roupe, K. A., & Yáñez, J. A. (2004). Cyclooxygenase-3: Axiom, dogma, anomaly, enigma or splice error? - Not as easy as 1, 2, 3. *Journal of Pharmacy and Pharmaceutical Sciences*, *7*(2), 217–226.

Dukes, G. E., Pharm, D., Sanders, S. W., Pharm, D., Russo, J., & Pharm, D. (2017). Transaminase Elevations in Patients Receiving Bovine or Porcine Heparin, (12), 646–650.

Edwards, I. R., & Aronson, J. K. (2000). Adverse drug reactions Adverse drug reactions : definitions , diagnosis , and management, *356*, 1255–1259.

Evans, D. C., Watt, A. P., Nicoll-griffith, D. A., & Baillie, T. A. (2004). Drug - Protein Adducts : An Industry Perspective on Minimizing the Potential for Drug Bioactivation in Drug Discovery and Development, 3–16.

Flavell, R. R., Truillet, C., Regan, M. K., Ganguly, T., Blecha, J. E., Kurhanewicz, J., … Wilson, D. M. (2016). Caged [18F]FDG Glycosylamines for Imaging Acidic Tumor

Microenvironments Using Positron Emission Tomography. *Bioconjugate Chemistry*, *27*(1), 170–178. https://doi.org/10.1021/acs.bioconjchem.5b00584

Golghalyani, V., Neupärtl, M., Wittig, I., Bahr, U., & Karas, M. (2017). ArgC-Like Digestion: Complementary or Alternative to Tryptic Digestion? *Journal of Proteome Research*, *16*(2), 978–987. https://doi.org/10.1021/acs.jproteome.6b00921

Hodgman, M. J., & Garrard, A. R. (2012). A Review of Acetaminophen Poisoning. *Critical Care Clinics*, *28*(4), 499–516. https://doi.org/10.1016/j.ccc.2012.07.006

Holt, M. P., & Ju, C. (2006). Mechanisms of drug-induced liver injury. *The AAPS Journal*, *8*(1), E48–E54. https://doi.org/10.1208/aapsj080106

Jullian, M., Hernandez, A., Maurras, A., Puget, K., Amblard, M., Martinez, J., & Subra, G. (2009). N-terminus FITC labeling of peptides on solid support: the truth behind the spacer. *Tetrahedron Letters*, *50*(3), 260–263. https://doi.org/10.1016/j.tetlet.2008.10.141

Khoury, T., Rmeileh, A. A., Yosha, L., Benson, A. A., Daher, S., & Mizrahi, M. (2015). Drug Induced Liver Injury: Review with a Focus on Genetic Factors, Tissue Diagnosis, and Treatment Options. *Journal of Clinical and Translational Hepatology*, *3*(2), 99–108. https://doi.org/10.14218/JCTH.2015.00007

Koen, Y. M., Liu, K., Shinogle, H., Williams, T. D., & Hanzlik, R. P. (2016). Comparative Toxicity and Metabolism of N - Acyl Homologues of Acetaminophen and Its Isomer 3 ′ - Hydroxyacetanilide. https://doi.org/10.1021/acs.chemrestox.6b00270

Koen, Y. M., Galeva, N. A., Metushi, I. G., Uetrecht, J., & Hanzlik, R. P. (2016). Protein Targets of Isoniazid-Reactive Metabolites in Mouse Liver in Vivo. *Chemical Research in Toxicology*, *29*(6), 1064–1072. https://doi.org/10.1021/acs.chemrestox.6b00098

Koen, Y. M., Galeva, N. A., Metushi, I. G., Uetrecht, J., & Hanzlik, R. P. (2016). Protein targets of isoniazid reactive metabolites in mouse liver in vivo. *Chemical Research in Toxicology*, acs.chemrestox.6b00098. https://doi.org/10.1021/acs.chemrestox.6b00098

Larson, A. M., Ii, T. J. D., Murray, N. G., Mccashland, T., & Reisch, J. S. (2009). Intravenous N -Acetylcysteine Improves Transplant-Free Survival in Early. *YGAST*, *137*(3), 856–864.e1. https://doi.org/10.1053/j.gastro.2009.06.006

Lee, M. H., Han, J. H., Kwon, P. S., Bhuniya, S., Kim, J. Y., Sessler, J. L., … Kim, J. S. (2012). Hepatocyte-targeting single galactose-appended naphthalimide: A tool for intracellular thiol imaging in vivo. *Journal of the American Chemical Society*, *134*(2), 1316–1322. https://doi.org/10.1021/ja210065g

Lee, S., Kang, S. W., Ryu, J. H., Na, J. H., Lee, D. E., Han, S. J., … Kim, K. (2014). Tumor-homing glycol chitosan-based optical/PET dual imaging nanoprobe for cancer diagnosis. *Bioconjugate Chemistry*, *25*(3), 601–610. https://doi.org/10.1021/bc500020g

Lee, Y. J., Kurra, Y., & Liu, W. R. (2016). Phospha-Michael Addition as a New Click Reaction for Protein Functionalization. *ChemBioChem*, *17*(6), 456–461. https://doi.org/10.1002/cbic.201500697

Leeming, M. G., Gamon, L. F., Wille, U., Donald, W. A., & O'Hair, R. A. J. (2015). What Are the Potential Sites of Protein Arylation by N-Acetyl-p-benzoquinone Imine (NAPQI)? *Chemical Research in Toxicology*, *28*(11), 2224–2233. https://doi.org/10.1021/acs.chemrestox.5b00373

Leise, M. D., Poterucha, J. J., & Talwalkar, J. A. (2014). Drug-Induced Liver Injury. *Mayo Clinic Proceedings*, *89*(1), 95–106. https://doi.org/http://dx.doi.org/10.1016/j.mayocp.2013.09.016

Leung, L., Kalgutkar, A. S., Obach, R. S., Leung, L., Kalgutkar, A. S., & Obach, R. S. (2017). Metabolic activation in drug-induced liver injury Metabolic activation in drug-induced liver injury, *2Leung*, *L.*(June). https://doi.org/10.3109/03602532.2011.605791

Lewis, J. H., & Stine, J. G. (2013). Review article: Prescribing medications in patients with cirrhosis - A practical guide. *Alimentary Pharmacology and Therapeutics*, *37*(12), 1132–1156. https://doi.org/10.1111/apt.12324

Lewis, J. H. (2015). The Art and Science of Diagnosing and Managing Drug-induced Liver Injury in 2015 and Beyond. *Clinical Gastroenterology and Hepatology*, *13*(12), 2173–2189.e8. https://doi.org/10.1016/j.cgh.2015.06.017

López-Alonso, J. P., Diez-García, F., Font, J., Ribó, M., Vilanova, M., Scholtz, J. M., … Laurents, D. V. (2009). Carbodiimide EDC induces cross-links that stabilize RNase a C-dimer against dissociation: EDC adducts can affect protein net charge, conformation, and activity. *Bioconjugate Chemistry*, *20*(8), 1459–1473. https://doi.org/10.1021/bc9001486

Maes, M., Vinken, M., & Jaeschke, H. (2016). Experimental models of hepatotoxicity related to acute liver failure. *Toxicology and Applied Pharmacology*, *290*, 86–97. https://doi.org/10.1016/j.taap.2015.11.016

Matthewsa, M., Hinson, J. A., Robertsa, D. W., & Pumford, N. R. (1997). Toxicology Letters Comparison of covalent binding of acetaminophen and the regioisomer 3 ' - hydroxyacetanilide to mouse liver protein, *4274*(96).

Mcmillan, H. J., Gregas, M., Darras, B. T., & Kang, P. B. (2011). Serum Transaminase Levels in Boys With Duchenne and Becker Muscular Dystrophy. https://doi.org/10.1542/peds.2010-0929

Meienhofer, J., & Trzeciak, A. (1971). Solid-Phase Synthesis with Attachment of Peptide to Resin through an Amino Acid Side Chain : [8-Lysine] -Vasopressin, *68*(5), 1006–1009.

Mitchell, J. R., Jollow, D. J., Potter, W. Z., Gillette, J. R., & Brodie, B. B. (1973). ROLE OF hepatic. *J. of Pharmacol. Exp. Ther.*, (187), 185–194.

Moser, M., Behnke, T., Hamers-Allin, C., Klein-Hartwig, K., Falkenhagen, J., & Resch-Genger, U. (2015). Quantification of PEG-Maleimide Ligands and Coupling Efficiencies on Nanoparticles with Ellman's Reagent. *Analytical Chemistry*, *87*(18), 9376–9383. https://doi.org/10.1021/acs.analchem.5b02173

Nathwani, R. A., Pais, S., Reynolds, T. B., & Kaplowitz, N. (2005). Serum Alanine Aminotransferase in, 1–3. https://doi.org/10.1002/hep.20548

Neve, R. M., Chin, K., Fridlyand, J., Yeh, J., Baehner, F. L., Fevr, T., … Gray, J. W. (2006). A collection of breast cancer cell lines for the study of functionally distinct cancer subtypes. *Cancer Cell*, *10*(6), 515–527. https://doi.org/10.1016/j.ccr.2006.10.008

Nossier, A. I., Eissa, S., Ismail, M. F., Hamdy, M. A., & Azzazy, H. M. E. S. (2014). Direct detection of hyaluronidase in urine using cationic gold nanoparticles: A potential diagnostic test for bladder cancer. *Biosensors and Bioelectronics*, *54*, 7–14. https://doi.org/10.1016/j.bios.2013.10.024

Offerman, S. R. (2011). The Clinical Management of Acetaminophen Poisoning in a Community Hospital System: Factors Associated with Hospital Length of Stay. *Journal of Medical Toxicology*, *7*(1), 4–11. https://doi.org/10.1007/s13181-010-0115-5

Ouellet, M., & Percival, M. D. (2001). Mechanism of Acetaminophen Inhibition of Cyclooxygenase Isoforms. *Archives of Biochemistry and Biophysics*, *387*(2), 273–280. https://doi.org/10.1006/abbi.2000.2232

Park, B. K., Boobis, A., Clarke, S., Goldring, C. E. P., Jones, D., Kenna, J. G., … Baillie, T. A. (2011). Managing the challenge of chemically reactive metabolites in drug development, *10*(April). https://doi.org/10.1038/nrd3408

Park, J. G., Langenwalter, K. J., Weinbaum, C. A., Casey, P. J., & Pang, Y. P. (2004). Improved loading and cleavage methods for solid-phase synthesis using chlorotrityl resins: Synthesis and testing of a library of 144 discrete chemicals as potential farnesyltransferase inhibitors. *Journal of Combinatorial Chemistry*, *6*(3), 407–413. https://doi.org/10.1021/cc0340729

Phan, J., Zdanov, A., Evdokimov, A. G., Tropea, J. E., Peters, H. K., Kapust, R. B., … Waugh, D. S. (2002). Structural basis for the substrate specificity of tobacco etch virus protease. *Journal of Biological Chemistry*, *277*(52), 50564–50572. https://doi.org/10.1074/jbc.M207224200

Prescott, L. (1980). Kinetics and metabolism of paracetamol and phenacetin. *British Journal of Clinical Pharmacology*, *10*(2 S), 291S–298S. https://doi.org/10.1111/j.1365-2125.1980.tb01812.x

Roberts, E. A. (2014). Drug-induced liver disease. *Liver Disease in Children*, *84*(5), 341–69. https://doi.org/10.1017/CBO9780511547409.022

Rutkowska, A., Thomson, D. W., Vappiani, J., Werner, T., Mueller, K. M., Dittus, L., … Bantscheff, M. (2016). A Modular Probe Strategy for Drug Localization, Target Identification and Target Occupancy Measurement on Single Cell Level. *ACS Chemical Biology*, *11*(9), 2541–2550. https://doi.org/10.1021/acschembio.6b00346

Ryan, M. D., & Flint, M. (1997). Virus-encoded proteinases of the picornavirus super-group. *Journal of General Virology*, *78*(4), 699–723. https://doi.org/10.1099/0022-1317-78-4-699

Schomaker, S., Warner, R., Bock, J., Johnson, K., Potter, D., Winkle, J. Van, & Aubrecht, J. (2013). Assessment of Emerging Biomarkers of Liver Injury in Human Subjects, *132*(2), 276–283. https://doi.org/10.1093/toxsci/kft009

Serrano, B. P., Szydlo, H. S., Alfandari, D. R., & Hardy, J. A. (2017). Active-site adjacent phosphorylation at Tyr-397 by c-Abl kinase inactivates caspase-9. *The Journal of Biological Chemistry*, jbc.M117.811976. https://doi.org/10.1074/jbc.M117.811976

Stamper, B. D., Mohar, I., Kavanagh, T. J., & Nelson, S. D. (2011). Proteomic analysis of acetaminophen-induced changes in mitochondrial protein expression using spectral counting. *Chemical Research in Toxicology*, *24*(4), 549–558. https://doi.org/10.1021/tx1004198

Stephen, C., & Lilly, E. (1968). WHICH ARE COMPATIBLE WITH N-a-CARBOBENZOXY PROTECTION, (11), 1297–1300.

Štimac, A., Šekutor, M., Mlinarić-Majerski, K., Frkanec, L., & Frkanec, R. (2017). Adamantane in Drug Delivery Systems and Surface Recognition. *Molecules*, *22*(2), 297. https://doi.org/10.3390/molecules22020297

Stine, J. G., Sateesh, P., & Lewis, J. H. (2013). Drug-induced liver injury in the elderly. *Current Gastroenterology Reports*, *15*(1). https://doi.org/10.1007/s11894-012-0299-8

Szumigala, R. H., Onofiok, E., Karady, S., Armstrong, J. D., & Miller, R. A. (2005). Mild non-transition metal catalyzed deprotection of N-allyloxycarbonyl amines. *Tetrahedron Letters*, *46*(25), 4403–4405. https://doi.org/10.1016/j.tetlet.2005.04.064

Uetrecht, J., & Naisbitt, D. J. (2013). Idiosyncratic Adverse Drug Reactions : Current Concepts, (April), 779–808.

Whitby, L. R., Obach, R. S., Simon, G. M., Hayward, M. M., & Cravatt, B. F. (2017). Quantitative Chemical Proteomic Pro fi ling of the in Vivo Targets of Reactive Drug Metabolites. https://doi.org/10.1021/acschembio.7b00346

Wilhelm, S., Tavares, A. J., Dai, Q., Ohta, S., Audet, J., Dvorak, H. F., … Watkins, J. C. (2016). Analysis of nanoparticle delivery to tumours. *Nature Reviews Materials*, *1*(5), 16014. https://doi.org/10.1038/natrevmats.2016.14

Yang, K., Battista, C., Woodhead, J. L., Stahl, S. H., Mettetal, J. T., Watkins, P. B., … Howell, B. A. (2017). Systems Pharmacology Modeling of Drug- induced Hyperbilirubinemia : Differentiating Hepatotoxicity and Inhibition of Enzymes / Transporters, *101*(4), 501–509. https://doi.org/10.1002/cpt.619

Zeng, X., Sun, Y.-X., Zhang, X.-Z., & Zhuo, R.-X. (2009). Biotinylated disulfide containing PEI/avidin bioconjugate shows specific enhanced transfection efficiency in HepG2 cells. *Organic & Biomolecular Chemistry*, *7*(20), 4201–10. https://doi.org/10.1039/b910831a

Zorn, C., Gnad, F., Salmen, S., & Reiser, O. (2001). Deprotection of N -Alloc amines by Pd (0) / DABCO — an efficient method for in situ peptide coupling of labile amino acids. *Tetrahedron Letters*, *42*, 7049–7053. https://doi.org/10.1016/S0040-4039(01)01453-8

Appendix I:

ROI Raw Data:

Gal-Gly IONP Raw Data

ROI	Patient	Series	Modality	Color	Voxels	Area mmÂ²	Mean	StdDev	Min	Max	Sum	Unit	Conc Peakm	Conc Max	Conc	Conc Unit
background	Gly-IONP 2		MR	transparent	130464	1791.67	465.435	469.402	0	3703.17	6.07E+07	UNK	95075.7	128407	33891.7	UNK/mmÂ²
background	Gly-IONP 2		MR	transparent	130464	1791.67	501.826	500.748	1	3976.27	6.55E+07	UNK	104070	137877	36541.6	UNK/mmÂ²
background	Gly-IONP 2		MR	transparent	130464	1791.67	439.574	427.315	2.74848	3833.3	5.73E+07	UNK	97797.4	132919	32008.5	UNK/mmÂ²
background	Gly-IONP 2		MR	transparent	130464	1791.67	495.704	485.343	3.75524	3943.28	6.47E+07	UNK	100488	136733	36095.7	UNK/mmÂ²
background	Gly-IONP 2		MR	transparent	130464	1791.67	481.641	469.066	2	3761.47	6.28E+07	UNK	98678.1	130428	35071.7	UNK/mmÂ²
background	Gly-IONP 2		MR	transparent	130464	1791.67	492.702	501.195	1	3869.46	6.43E+07	UNK	99521.6	134173	35877.2	UNK/mmÂ²
background	Gly-IONP 2		MR	transparent	130464	1791.67	398.746	409.715	0	3772.56	5.20E+07	UNK	97532.5	130813	29035.5	UNK/mmÂ²
background	Gly-IONP 2		MR	transparent	130464	1791.67	423.785	434.903	1.49897	3946.28	5.53E+07	UNK	102462	136836	30858.8	UNK/mmÂ²
background	Gly-IONP 2		MR	transparent	130464	1791.67	404.812	403.235	0	3952.23	5.28E+07	UNK	103765	137043	29477.3	UNK/mmÂ²
background	Gly-IONP 2		MR	transparent	130464	1791.67	374.164	387.768	0.75139	3717.19	4.88E+07	UNK	98168.9	128893	27245.5	UNK/mmÂ²
Liver	Gly-IONP 2		MR	red	608	8.34968	565.087	114.558	332.001	1010.76	343573	UNK	32161.9	35047.8	41148	UNK/mmÂ²
Liver	Gly-IONP 2		MR	red	608	8.34968	460.452	128.723	220.501	968.508	279955	UNK	27988.1	33582.9	33528.8	UNK/mmÂ²
Liver	Gly-IONP 2		MR	red	608	8.34968	336.507	131.362	58.2519	818.012	204596	UNK	23854.8	28364.4	24503.5	UNK/mmÂ²
Liver	Gly-IONP 2		MR	red	608	8.34968	401.841	152.69	100	1154.25	244320	UNK	34057.8	40023.5	29260.9	UNK/mmÂ²
Liver	Gly-IONP 2		MR	red	608	8.34968	378.487	143.436	110.25	1046	230120	UNK	29151.4	36270	27560.3	UNK/mmÂ²
Liver	Gly-IONP 2		MR	red	608	8.34968	377.115	116.952	128	764.009	229286	UNK	22501.3	26491.9	27460.4	UNK/mmÂ²
Liver	Gly-IONP 2		MR	red	608	8.34968	302.891	98.9762	67.7501	675.252	184158	UNK	21458.6	23414.2	22055.7	UNK/mmÂ²
Liver	Gly-IONP 2		MR	red	608	8.34968	340.744	99.4207	98.7495	670.253	207173	UNK	17464.7	23240.9	24812	UNK/mmÂ²
Liver	Gly-IONP 2		MR	red	608	8.34968	310.148	88.3743	70.7477	666.75	188570	UNK	19891.8	23119.4	22584.1	UNK/mmÂ²
Liver	Gly-IONP 2		MR	red	608	8.34968	269.308	79.5042	101	631.25	163739	UNK	19428	21888.5	19610.3	UNK/mmÂ²

CMX-IONP Raw Data

ROI	Patient	Series	Modality	Color	Voxels	Area mmå_	Mean	StdDev	Min	Max	Sum	Unit	Conc Peakmå	Conc Max	Conc	Conc Unit
background	CMX-IONP		MR	transparent	128020	1758.1	451.155	467.328	0	2618.74	5.78E+07	UNK	84777	90804.4	32851.8	UNK/mmå_
background	CMX-IONP		MR	transparent	128020	1758.1	411.871	446.612	1.7514	2727.96	5.27E+07	UNK	92300	94591.6	29991.3	UNK/mmå_
background	CMX-IONP		MR	transparent	128020	1758.1	418.592	447.638	0.249547	2549.9	5.36E+07	UNK	83808.3	88417.4	30480.7	UNK/mmå_
background	CMX-IONP		MR	transparent	128020	1758.1	416.388	438.64	0.751581	2427.24	5.33E+07	UNK	80960.8	84164	30320.2	UNK/mmå_
background	CMX-IONP		MR	transparent	128020	1758.1	385.158	406.49	0.998207	2314.78	4.93E+07	UNK	75331.7	80264.7	28046.1	UNK/mmå_
background	CMX-IONP		MR	transparent	128020	1758.1	363.041	364.317	0.498941	2025.48	4.65E+07	UNK	63814.5	70233	26435.6	UNK/mmå_
background	CMX-IONP		MR	transparent	128020	1758.1	399.289	398.275	1.75125	2338.53	5.11E+07	UNK	74329.6	81088	29075.1	UNK/mmå_
background	CMX-IONP		MR	transparent	128020	1758.1	369.218	360.681	1	2128.3	4.73E+07	UNK	67185.8	73798.6	26885.4	UNK/mmå_
background	CMX-IONP		MR	transparent	128020	1758.1	369.218	360.681	1	2128.3	4.73E+07	UNK	67185.8	73798.6	26885.4	UNK/mmå_
background	CMX-IONP		MR	transparent	128020	1758.1	424.764	448.408	0.998121	2742.04	5.44E+07	UNK	84836.5	95079.9	30930.1	UNK/mmå_
background	CMX-IONP		MR	transparent	128020	1758.1	316.685	319.783	1	1901.24	4.05E+07	UNK	59316.3	65925.3	23060.1	UNK/mmå_
liver	CMX-IONP		MR	red	3052	41.9132	425.491	153.828	50.5023	1684.53	1.30E+06	UNK	43007.3	58410.8	30983	UNK/mmå_
liver	CMX-IONP		MR	red	3052	41.9132	168.995	111.076	6.25083	939.992	515774	UNK	23984.9	32594.1	12305.8	UNK/mmå_
liver	CMX-IONP		MR	red	3052	41.9132	252.252	121.206	20.2486	1141.26	769873	UNK	30776.8	39573.2	18368.3	UNK/mmå_
liver	CMX-IONP		MR	red	3052	41.9132	279.384	156.954	18.2505	1314.01	852679	UNK	35905.8	45563.1	20343.9	UNK/mmå_
liver	CMX-IONP		MR	red	3052	41.9132	215.631	121.654	17.2479	1026	658105	UNK	27102.8	35576.3	15701.6	UNK/mmå_
liver	CMX-IONP		MR	red	3052	41.9132	254.326	122.67	12.5005	853.499	776203	UNK	25834.4	29594.9	18519.3	UNK/mmå_
liver	CMX-IONP		MR	red	3052	41.9132	187.965	114.877	12.9986	1075.26	573670	UNK	29873.9	37284.4	13687.1	UNK/mmå_
liver	CMX-IONP		MR	red	3052	41.9132	302.113	144.747	22.2468	750.008	922048	UNK	24082.6	26006.4	21999	UNK/mmå_
liver	CMX-IONP		MR	red	3052	41.9132	302.113	144.747	22.2468	750.008	922048	UNK	24082.6	26006.4	21999	UNK/mmå_
liver	CMX-IONP		MR	red	3052	41.9132	259.489	153.385	6.24938	1237.51	791959	UNK	35401.6	42910.4	18895.2	UNK/mmå_
liver	CMX-IONP		MR	red	3052	41.9132	226.75	150.944	11.25	864.246	692040	UNK	26834.6	29967.6	16511.3	UNK/mmå_